Journal of Catalysis 370 (2019) 186–199

Contents lists available at ScienceDirect

Journal of Catalysis

journal homepage: www.elsevier.com/locate/jcat

Mechanistic details of C—O bond activation in and H-addition to guaiacol at water-Ru cluster interfaces

Junnan Shangguan, Niklas Pfriem, Ya-Huei (Cathy) Chin *

Department of Chemical Engineering and Applied Chemistry, University of Toronto, Toronto, Canada

ARTICLE INFO

Article history:
Received 19 August 2018
Revised 15 November 2018
Accepted 26 November 2018

Keywords:
Guaiacol hydrodeoxygenation
Phenolic compound
Ruthenium
Aqueous phase catalysis
Hydrogenation
H-addition
C—O bond activation
Deuterium labeling
Isotopic exchange

ABSTRACT

Catalytic pathways of guaiacol and hydrogen (H_2) reactions on dispersed Ru clusters in the aqueous medium and the associated kinetic requirements for C—OCH_3 bond cleavage and H-addition steps are established based on kinetic and isotopic investigations. Time-dependent kinetic measurements in a gradientless semi-batch reactor reveal that guaiacol reacts with H_2 via two independent routes of C—OCH_3 bond cleavage and H-addition; the former leads to phenol, cyclohexanone, cyclohexanol, and cyclohexane and latter to 2-methoxy-cyclohexanol. During catalysis, an adsorbed guaiacol undergoes a single, quasi-equilibrated H-adatom (H^*) addition on its aromatic ring, forming a partially-hydrogenated intermediate, before the sequential kinetically relevant C—OCH_3 cleavage or H^* addition steps on Ru cluster surfaces nearly saturated with deprotonated guaiacol. Increasing the H^* coverage promotes the overall turnovers but decreases the selectivity towards the C—OCH_3 bond cleavage, because H^* addition event not only activates guaiacol but also promotes H-addition without breaking its C—O bond.

1. Introduction

Catalytic transformation of phenolic monomers (phenol, anisole, catechol, and guaiacol) in lignin to cyclic hydrocarbons is an attractive route for synthesizing sustainable chemical feedstocks [1–4]. Among the various phenolic monomers, guaiacol is structurally most complex, as it contains an aryl ether (Ar—OCH_3) and a phenolic hydroxyl (Ar—OH) linkages. Scheme 1 shows the structure of a guaiacol, which contains six aromatic carbons (C^1—C^6) and one aliphatic carbon (C^7). Carbon atom C^1 connects to a hydroxyl group (C^1—OH), C^2 to a methoxy group, and C^3, C^4, C^5, and C^6 each connects to an H-atom (C^a—H, $a = 3$–6). C^7 is the only aliphatic carbon that bonds to an oxygen atom and three H-atoms (H_3C^7—OC^2). There are three C—O bonds in guaiacol, namely C^1—OH, C^7—OC^2, and C^2—OC^7 bonds. Hydrodeoxygenation of guaiacol involves cleaving some or all of these C—O bond(s), which may occur either concomitantly or in sequence via multiple pathways. Scheme 1a summarizes the plausible primary hydrodeoxygenation pathways for guaiacol-H_2 reactions on transition metal catalysts. Taking Ru as an example, hydrogen addition onto the benzylic ring forms 2-methoxy-cyclohexanol [5,6], hydrogenolysis of C^1—OH bond to anisole [7,8], hydrogenolysis of C^2—OC^7 bond to phenol [5,7,8], and hydrogenolysis of C^7—OC^2 bond to catechol [8]. The primary products may undergo secondary hydrodeoxygenation, producing cycloalkanes and cycloalkanols. As illustrated in Scheme 1b, hydrogenation of phenol with its C—O bond intact forms cyclohexanone then cyclohexanol (Pathways 2 and 3), and alternatively hydrogenation with its C—O bond cleaved forms cyclohexane (Pathway 4) [9–11].

This complex reaction network (Scheme 1) has brought forth significant challenges in probing the individual reaction paths, even for reactions at the vapor-metal interface without solvent molecules, at which the solvation effects are do not exist [6–8,12–14]. In the presence of a solvent, the solvation effects may influence the energies of the reactants, intermediates, and transition states along the catalytic paths and, in turn, the catalytic sequences, rates, and selectivities. Despite extensive studies on this reaction system and a wealth of conversion and selectivity data generated for this reaction at both the vapor-Ru [6–8,12–14] and water-Ru [5,15,16] interfaces, there is a lack of detailed kinetic assessments and mechanistic interpretation, specifically, on the reaction network, reversibilities of the individual reaction steps, interdependencies of the reaction paths, and the identity of most abundant surface intermediates and kinetically relevant steps. Previous studies have reported the apparent activation barrier, reaction pathways, and first-order rate constants for guaiacol (0.8 M) and H_2 (2 bar) reactions at 453–513 K on bi-functional

---

* Corresponding author.
E-mail address: cathy.chin@utoronto.ca (Y.-H. Chin).

https://doi.org/10.1016/j.jcat.2018.11.036

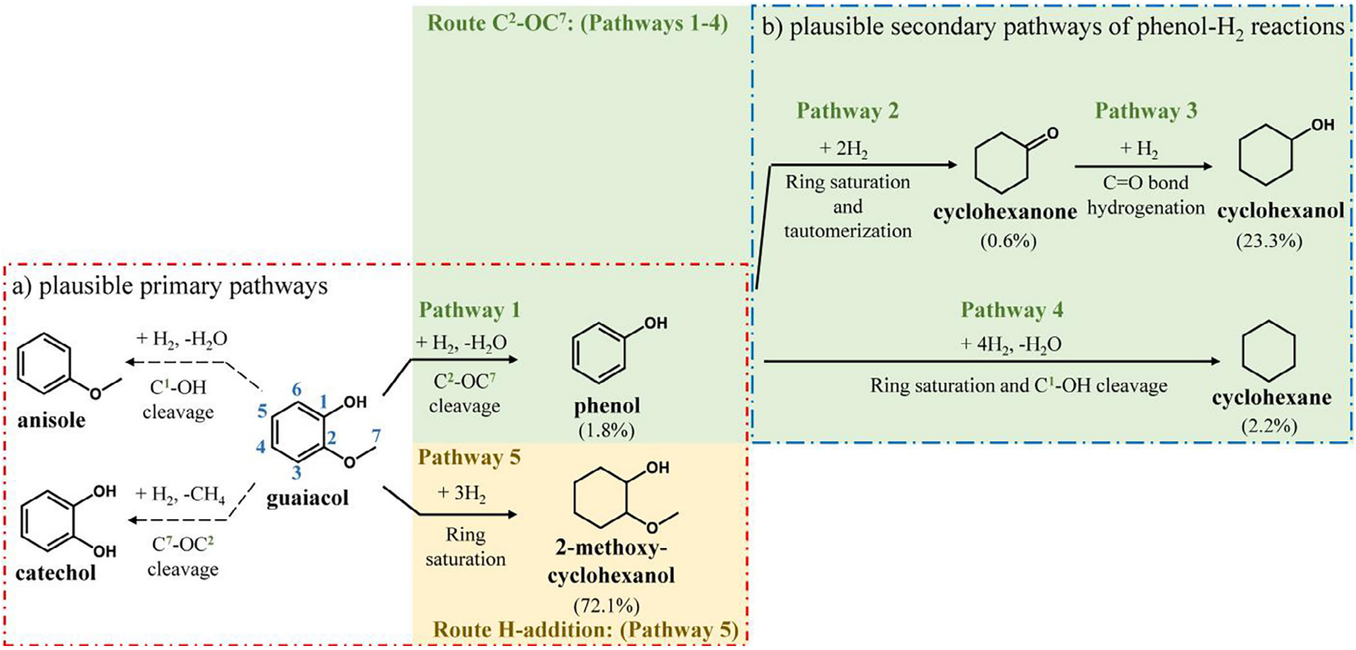

Scheme 1. A comprehensive reaction network of guaiacol-H_2 reactions, which includes (1a) plausible primary hydrodeoxygenation pathways and (1b) plausible secondary reaction pathways starting from phenol intermediates (Pathways 2–4). [– – –▸ denotes a catalytically inconsequential pathway, whereas ——▸ denotes a catalytically consequential pathway (details analyses in Section 3.1).]

Ru/H-ZSM-5 catalysts with water solvent [17]. However, an explanation on the exact functionalities of Ru cluster surfaces and solid acids, kinetic dependencies on guaiacol and H_2, catalytic role of reactive hydrogen species, coverages and identity of the various intermediates, and a link between these catalytic events and elementary steps to the observed rate dependencies have remained largely missing. Literature has reported the selectivities towards C—O bond cleavage (mainly as cyclohexanol) and H-addition (as 2-methoxy-cyclohexanol) products of ~75% and ~25%, respectively, during guaiacol (1 M) and H_2 (40 bar) reactions on Ru-H_2O interface at 523 K [5]. However, the apparent selectivity dependencies on H_2 pressure and guaiacol concentration and the specific elementary steps leading to such dependencies are unclear.

In terms of theory, density functional theory (DFT) calculations have examined somewhat extensively the reactions on transition metal surfaces {Pt(1 1 1) [18,19], Ru(0 0 0 1) [20,21], Fe(1 1 0) [22], and Pd(1 1 1) [22]}. These studies, however, predominantly focus on model surfaces largely free of adsorbates and in vacuum, without solvent molecules. Their findings, especially on the most preferred reaction path(s), may not translate directly to the reaction events occurred at the water-metal interfaces, at which the interactions between water solvent molecules and reactive fragments, including the transition states, and among the water molecules do matter. These additional interactions influence the energies of the adsorbed reactants, intermediates, transition states, and products along the reaction coordinate to different extents [23,24] and, in turn, mediate the rates and selectivities.

Here, we establish the reaction network for guaiacol-H_2 reactions at the water-Ru cluster interface with rigorous rate assessments, kinetic modeling, and H-D isotopic exchange studies and explain the mechanistic requirements for the two competing routes of C^2—OC^7 bond cleavage and H-addition. These experimental findings, together with the adsorption configurations and energies of the various reactive fragments derived from DFT calculations [21], led to a proposed sequence of catalytic events. Guaiacol adsorbs on an ensemble of Ru sites and reacts with chemisorbed H-adatoms (H^*) via a single, rapid, quasi-equilibrated H-addition event onto its benzylic ring, forming a partially-hydrogenated guaiacol as the common reactive intermediate. This intermediate undergoes an irreversible, kinetically relevant C^2—OC^7 bond cleavage step, when a vicinal Ru site is available, forming phenol, cyclohexanone, cyclohexanol, and cyclohexane. Alternatively, it undergoes the competing, irreversible, kinetically-relevant H-addition step with a neighboring hydrogen adatom (H^*), forming 2-methoxy-cyclohexanol after a series of successive hydrogen addition events. Because of the different site requirements, namely vacancy site (*) versus H-adatom (H^*), of the C^2—OC^7 bond cleavage and H-addition routes, respectively, the selectivity towards the desired C^2—OC^7 bond cleavage products increases with increasing vacancy-to-hydrogen adatom site ratio (*-to-H^*), as dictated by the inverse square root of H_2 pressure. H-D isotopic exchanges on C^3, C^4, C^5, or C^6 during guaiacol-H_2-D_2O reactions confirm that the first H^* addition onto one of these carbon atoms of guaiacol is reversible, as the ring deuterated guaiacol forms and accumulates prior to its sequential hydrodeoxygenation reactions. The mechanistic framework established here describes the formation of a common, partially hydrogenated guaiacol-derived intermediate, site requirements of C^2—OC^7 bond cleavage and H-addition routes, and how H_2 pressure influences the vacancy-to-hydrogen adatom coverage ratio and in turn the selectivities during guaiacol hydrodeoxygenation.

2. Experimental methods

2.1. Preparation and characterizations of dispersed Ru clusters supported on activated carbon powders

Activated carbon powders (Norit, Activated Carbon, SX ULTRA CAT 8020-1, surface area of 1200 $m^2\ g^{-1}$, pore volume of 1.4 cm^3 -g^{-1}, 90% of the mean particle size are < 100 μm) were placed in a quartz boat and treated in a furnace under flowing He (Linde certified standard, 99.999%, 0.2 $cm^3\ g^{-1}\ s^{-1}$), by increasing the temperature (0.03 K s^{-1}) to 573 K, holding for 7 h, and then cooling to 298 K. Ruthenium (1 wt%) was incorporated into the treated carbon powders by incipient wetness impregnation method, by adding an aqueous $Ru(NO)(NO_3)_3$ solution, prepared from mixing $Ru(NO)(NO_3)_3$ (Sigma Aldrich, 1.4 wt% Ru, CAS Number: 34513-98-9) with doubly-deionized water (>18 MΩ cm), onto the carbon powders in a drop-wise manner. After the impregnation step, the sample was aged in the ambient environment for 12 h, dried at 348 K for another 12 h, then treated under flowing 5% H_2/He (Linde certified standard, $0.4\ cm^3\ g^{-1}\ s^{-1}$) by heating at $0.16\ K\ s^{-1}$ to 723 K, maintaining isothermally at 723 K for 5 h, and then cooling to the ambient temperature ($\sim 0.08\ K\ s^{-1}$). A flowing stream of He (Linde certified standard, 99.999%, $0.2\ cm^3\ g^{-1}\ s^{-1}$) was introduced to remove any residue H_2 from the sample chamber. After that, a stream of 5.5% O_2/He (Linde certified standard, $0.1\ cm^3\ g^{-1}\ s^{-1}$) was introduced, which passivated the Ru clusters, before exposure of the prepared catalyst sample to the ambient air.

The average Ru cluster diameter and dispersion were determined from chemisorbed hydrogen uptakes, measured using a volumetric adsorption-desorption apparatus over 0–13 kPa H_2 at 313 K. The catalyst was first treated *in-situ* under flowing H_2 (Linde certified standard, 99.999%, $0.4\ cm^3\ g^{-1}\ s^{-1}$) by heating at $0.03\ K\ s^{-1}$ from ambient temperature to 573 K, holding isothermally at 573 K for 1 h, then exposing to the dynamic vacuum ($<5 \times 10^{-2}$ Pa) for 12 h at 573 K, and finally cooling to 313 K ($\sim 0.08\ K\ s^{-1}$) for the H_2 uptake measurements. Two sets of H_2 uptakes were carried out isothermally at 313 K and, between each set of the uptake measurements, the catalyst was exposed to dynamic vacuum ($<5 \times 10^{-2}$ Pa) for 30 min. The amount of chemisorbed hydrogen was determined by the difference in H/Ru ratios between the two H_2 uptake values at zero pressure, obtained by extrapolating the H/Ru ratios at higher pressures, at which the H/Ru ratios reached a plateau, to zero pressure. This value was used to estimate the Ru dispersion by assuming a H/Ru ratio of unity. The mean Ru cluster diameter was estimated from Ru dispersion, by assuming spherical structure with the volume occupied by surface Ru atom identical to that of Ru bulk of $13.65 \times 10^{-3}\ nm^3$ [25]. The dispersion value was 6% and the mean cluster size was 14 nm.

2.2. Rate and selectivity assessments with an isothermal, gradientless semi-batch stirred tank reactor

Rates and selectivities of guaiacol-H_2-H_2O reactions were measured with an isothermal, gradientless stirred tank reactor ($300\ cm^3$, Parr Instrument 4560 Mini Bench Top Reactors, Hastelloy) equipped with a mechanical propeller stirrer. The reactor was operated in a semi-batch mode with periodic sampling. Prior to guaiacol introduction, the tank was first filled with $100\ cm^3$ of doubly-deionized water (>18 MΩ cm) and 10–100 mg catalyst powders (1 wt% Ru/C). Air in the reactor was removed by purging with He (Linde certified standard, 99.999%, $>1.4\ cm^3\ s^{-1}$) for >120 s before charging the reactor with H_2 to 50 bar (at ambient temperature, Linde certified standard, 99.999%, $\sim 200\ cm^3$ in the reactor). The reactor was sealed, heated to 423 K, and then kept isothermally at 423 K while agitating at 900 rpm for at least 0.5 h for treating the Ru catalyst. The tank was then cooled to ambient temperature (298 K, $\sim 1.41\ K\ s^{-1}$) by applying ice-water bath and then depressurized to ambient pressure. Guaiacol (50–1000 mg, 99.5%, Sigma Aldrich), gas phase internal standard (propane, Linde, 99.0%, 0.76 bar at ambient temperature), and H_2 (10–55 bar, $\sim 200\ cm^3$ at ambient temperature, Linde certified standard, 99.999%) were added before heating the reactor up to 423 K ($\sim 0.24\ K\ s^{-1}$), the reaction temperature. Reaction time zero ($t = 0$) was defined at which the targeted reaction temperature was reached, right before the agitation started. The agitation speed was set at 900 rpm throughout a specific reaction time (0.25–1.00 h), because this agitation speed was above the 700 rpm, the agitation speed that has been confirmed to be free of temperature and concentration gradients and transport limitations for the case of phenol-H_2 reactions [26], occurred at rates much higher than the current study ($4.2 \times 10^{-3}\ mol_{phenol} \cdot h^{-1}$ and $\sim 3\ mol_{H_2} \cdot h^{-1}$ for phenol-H_2 vs. $\sim 2.4 \times 10^{-3}\ h^{-1}\ mol_{guaiacol} \cdot h^{-1}$ and $\sim 7.2 \times 10^{-3}\ mol_{H_2} \cdot h^{-1}$ for guaiacol-H_2) at comparable temperature (433–473 K). Upon reaching the targeted reaction time, the reactor tank was quenched from the reaction temperature to ambient temperature (298 K, $\sim 1.41\ K\ s^{-1}$), by immersing the tank into an ice-water bath. Gas phase samples were collected by connecting the reactor outlet to a gas chromatograph (Agilent 7890 A).

A small fraction of liquid was sampled from a liquid sampling port, which was made out of a dip-tube immersed in the liquid reaction mixture. The liquid sample was filtrated with a syringe filter (VWR, 0.2 μm polypropylene membrane), after which an internal standard ($\sim 0.02\ cm^3$ cyclopentanol, Sigma Aldrich 99.5%) was added to the sample, prior to its quantification. The reactants and products in the gas and liquid phases were quantified using a gas chromatograph (Agilent 7890 A) equipped with a flame ionization detector (FID) and a thermal conductivity detector (TCD). The FID is connected to a DB-1 column (30 m × 320 μm × 1 μm) for the quantification of products with C-H bond(s), whereas the TCD is connected to a Supel-Q column (30 m × 530 μm × 1 μm) for the quantifications of CO_x ($x = 1$ or 2).

Time-dependent concentration profiles during guaiacol-H_2-H_2O reactions were measured with the reactor configurations and start-up procedure described above, except that the reactor was quenched down from the isobaric (<0.2 bar pressure variations) and isothermal (at 423 K) reaction condition to the ambient temperature periodically (0.25–1.00 h) for the sampling of the gas and liquid phases following the methods described above. After sampling, the reactor was recharged at the ambient temperature with H_2 and propane (the gas phase internal standard) to pressures identical to those at the initial condition. This reactor operation mode, which involved time-dependent reaction, sampling, and recharging, together with controlling the reaction time between each sampling period such that H_2 consumption was minimized, ensured that the H_2 pressure was kept essentially constant and independent of the reaction time (varied by less than ±0.1 bar). Between each sampling period, the H_2 conversion was below 0.2%. After the periodic sampling, the reactor was heated up to the reaction temperature (423 K), before stirring at 900 rpm. Time-of-reaction (t) is defined as the duration at which the reactor remained at isobaric and isothermal conditions, while stirring with a constant agitation speed (900 rpm). The duration of gas/liquid sampling at ambient temperature, of re-introduction of H_2 and propane, and of reactor heating up and quenching down is excluded and not considered as a part of the time-of-reaction.

Product distributions and formation rates during guaiacol (4.9×10^{-2} M)-D_2O ($\sim 168\ cm^3$, 99.9 atom% D, Sigma Aldrich)–H_2 (30 bar, at 298 K, Linde certified standard, 99.999%, $\sim 132\ cm^3$ in the reactor, H_2-to-D_2O molar ratio of 0.017) on 10 mg Ru/C catalyst were measured with the reactor configurations and start-up procedure described above. The isotopic distributions of reactant and products were quantified by GC-MS (Agilent 7890 A and 5975C), first by chromatographic separation with a HP-5 ms capillary column (Agilent, 19091J-413, 30 m × 320 μm × 0.25 μm) followed by quantification with a mass selective detector (MSD) (Agilent 5975C).

3. Results and discussion

In what follows, we first identify the primary and secondary reaction pathways and simplify the reaction network (Scheme 1) by examining the initial rates and selectivities during the reactions of guaiacol or the potential primary and secondary products with

Table 1
Summary of conversions, turnover rates (*TOR*), and ring product selectivities during reactions of guaiacol and guaiacol-related compounds with 30 bar H_2 in the aqueous phase on Ru clusters at 423 K.

Entry	Ring reactant	Other reactant (s)	Ring reactant concentration (M)	Catalyst (mg)	Time (h)	Conversion (%)	TOR_i[a]	k_i^{1st}[b]	Ring product selectvities (%)								
									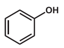	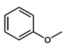	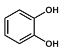	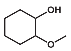	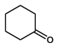	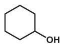	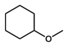	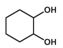	
1	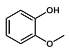	H_2—H_2O	4.1×10^{-2}	10	1	19.2	7.8×10^3	1.9×10^5	1.8	N.D.	N.D.	72.1	0.6	23.3	N.D.	N.D.	2.2
2	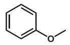	H_2—H_2O	4.6×10^{-2}	5	0.5	12.0	2.2×10^4	4.8×10^5	N.D.	–	–	–	N.D.	25.8	68.9	–	4.7
3	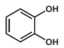	H_2—H_2O	4.6×10^{-2}	30	2	28.6	2.1×10^3	4.6×10^4	N.D.	–	–	–	N.D.	14.7	–	83.0	2.3
4	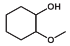	H_2—H_2O	0.3×10^{-2}	10	9	0.0	0.0	0.0	–	–	–	–	–	–	–	–	–
5	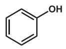	H_2—H_2O	5.4×10^{-2}	10	1	42.7	2.4×10^4	4.4×10^5	–	–	–	–	N.D.	96.3	–	–	3.2
6	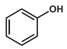	CH_3OH—H_2—H_2O	1.4×10^{-2}	10	4	99.9	$>5.6\times10^3$	4.0×10^5	–	N.D.	N.D.	N.D.	N.D.	95.4	N.D.	N.D.	4.6
7	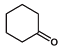	H_2—H_2O	4.6×10^{-2}	10	1	99.9	$>7.7\times10^4$	1.7×10^6	N.D.	–	N.D.	–	–	100	N.D.	N.D.	N.D.
8	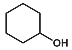	H_2—H_2O	4.0×10^{-2}	10	14.5	0.0	7.0×10^{-1}	1.8×10^1	–	–	–	–	–	–	–	–	100
9		H_2—H_2O	4.0×10^{-3}	10	5	0.0	0.0	0.0	N.D.	–	N.D.	–	N.D.	N.D.	–	N.D.	–

[a] Initial turnover rate of compound A, TOR_A, has a unit of $mol_A\cdot(mol_{Ru,surf}\cdot h)^{-1}$ (*A* = guaiacol, 2-methoxy-cyclohexanol, anisole, catechol, phenol, phenol-CH_3OH, cyclohexanone, cyclohexanol, or cyclohexane).
[b] Pseudo first-order rate constant, k_A^{1st}, is calculated as the ratio of TOR_A to the initial concentration of *A* and has a unit of $L\cdot(mol_{Ru,surf}\cdot h)^{-1}$.
Note: N.D. denotes non-detectable.

H_2 at the interface of water and Ru in Section 3.1; we then systematically examine the time-dependent product formation profiles during guaiacol-H_2 reactions on Ru clusters in the aqueous phase, apply kinetic analyses, and extract from which the effective reaction orders in Section 3.2. We propose a sequence of surface elementary reaction steps that demonstrates the catalytic significance of initial, quasi-equilibrated H-adatom addition in activating guaiacol molecule and initiating sequential hydrodeoxygenation reactions in Section 3.3, which is consistent with the effective kinetic dependencies of guaiacol and H_2. Finally, we confirm the reversibility of surface H-adatom addition events with H-D exchange at the aromatic ring of guaiacol with isotopic labeling experiments, as shown in Section 3.4.

3.1. Catalytic pathways for guaiacol-hydrogen reactions at water-Ru cluster interfaces

Table 1 compares the turnover rates (per exposed Ru atom), first-order rate constants, and product distributions during the reactions of hydrogen with reactants, intermediates, or products of guaiacol-H_2 reactions on 1 wt% Ru/C in the aqueous medium at 423 K and 30 bar H_2. Guaiacol-H_2 reactions produce 2-methoxy-cyclohexanol (72.1% selectivity) and, to smaller extents, phenol, cyclohexanone, cyclohexanol, and cyclohexane (1.8%, 0.6%, 23.3%, and 2.2% selectivities, respectively), as shown in Entry 1 of Table 1.

Anisole and catechol are potential primary products from C^1—OH and C^7—OC^2 bond cleavages, respectively, as shown in Scheme 1a, but they remain undetectable during guaiacol-H_2 reactions (Entry 1). A separate reaction of anisole with H_2 shows much higher reactivities comparing to that of guaiacol with H_2, and the first-order rate constant ratio for anisole-to-guaiacol, $k_{anisole}^{1st}\left(k_{guaiacol}^{1st}\right)^{-1}$, is 2.5 at 423 K (Entry 2 vs. Entry 1); the reaction forms methoxy-cyclohexane, cyclohexane, and cyclohexanol, at 68.9%, 4.7%, and 25.8% selectivities, respectively. This means that anisole, if formed as a primary product from guaiacol-H_2 reactions, must convert readily to produce mostly methoxy-cyclohexane. On the contrary, catechol, another potential primary product, reacts with H_2 at rates that are slower than guaiacol, and the first-order rate constant ratio for catechol-to-guaiacol, $k_{catechol}^{1st}\left(k_{guaiacol}^{1st}\right)^{-1}$, is 0.24 at 423 K (Entry 3 vs. Entry 1); the reactions form 1,2-cyclohexanediol, cyclohexanol, and cyclohexane at selectivities of 83.0%, 14.7%, and 2.3%, respectively. Thus, catechol, if formed as a primary product from guaiacol-H_2 reactions, must remain detectable, and a portion of which converts to 1,2-cyclohexanediol. Since guaiacol-H_2 reactions form neither anisole, methoxy-cyclohexane, catechol, nor 1,2-cyclohexanediol, both the C^1-OH and C^7-OC^2 hydrogenolysis reactions must be kinetically inconsequential.

2-Methoxy-cyclohexanol and phenol are the two detectable primary products (Scheme 1a) in guaiacol-H_2 reactions (Entry 1). 2-Methoxy-cyclohexanol does not react with H_2 (Entry 4); thus, it remains as a stable product during guaiacol-H_2 reactions without further conversion. In contrast, phenol reacts with H_2 much more rapidly with a first-order rate constant ratio for phenol-to-guaiacol, $k_{phenol}^{1st}\left(k_{guaiacol}^{1st}\right)^{-1}$, of 2.3 at 423 K (Entry 5 vs. Entry 1), forming predominantly cyclohexanol (96.3% selectivity) and a small amount of cyclohexane (3.2% selectivity). These are also the products observed during guaiacol-H_2 reactions. We note that cyclohexanone, a potential intermediate of phenol-H_2 reaction, remains undetected in phenol-H_2 reaction (Entry 5). Separate cyclohexanone-H_2 reactions (Entry 7) reveal that cyclohexanone hydrogenates much faster than phenol; in fact, cyclohexanone converts completely to cyclohexanol, and the first-order rate constant ratio for cyclohexanone-to-phenol, $k^{\mathrm{1st}}_{\mathrm{cyclohexanone}}\left(k^{\mathrm{1st}}_{\mathrm{phenol}}\right)^{-1}$, is estimated to be larger than 3.9 at 423 K (Entry 7 vs. Entry 5). Therefore, any cyclohexanone formed in phenol-H_2 reactions would convert completely to cyclohexanol.

Taken together the rate constants, their ratios, and the relative reactivities of guaiacol and its intermediate products, we conclude that guaiacol-H_2 reactions occur via two independent and competing reaction routes, as depicted in Scheme 1b, of (i) **Route $\mathbf{C^2—OC^7}$** that involves an initial $C^2—OC^7$ cleavage to phenol (**Pathway 1**), followed by either phenol hydrogenation to cyclohexanone (**Pathway 2**) and then to cyclohexanol (**Pathway 3**) or phenol hydrodeoxygenation to cyclohexane (**Pathway 4**) and (ii) **Route H-addition** that involves the direct hydrogenation of guaiacol to 2-methoxy-cyclohexanol (**Pathway 5**).

Next, we probe the reversibilities of these reactions (**Pathways 1–5**), by carrying out reactions between one of these reactants, i.e., phenol-CH_3OH, cyclohexanone, cyclohexanol, or cyclohexane, and H_2 on the same catalysts at similar reaction conditions (423 K, 30 bar H_2). Entries 6–9 in Table 1 summarize the product distributions and rate constant ratios of these studies. Incorporating methanol, the product of guaiacol-H_2 reaction via $C^2—OC^7$ bond cleavage (**Pathway 1**), into a phenol-H_2 reactant mixture does not lead to guaiacol or 2-methoxy-cyclohexanol. Instead, it produces cyclohexanol and cyclohexane, which are also the products of phenol-H_2 reactions (Entries 6 and 5). These results, taken together with the fact that 2-methoxy-cyclohexanol does not react with H_2 under these conditions (Entry 2), confirm that the primary $C^2—OC^7$ bond cleavage and H-addition pathways (**Pathways 1 and 5**) are irreversible. The cyclohexanone-H_2 and cyclohexane-H_2 reactions do not form phenol and cyclohexanol-H_2 reactions form neither cyclohexanone nor phenol, as shown in Entries 7–9. Therefore, these secondary pathways (**Pathways 2–4**) are also irreversible.

Since all primary and secondary pathways are irreversible, we can lump the site-time-yields (per Ru surface atom) of product *P* (denoted as STY_P, where *P* = phenol, cyclohexanone, cyclohexanol, cyclohexane, or 2-methoxy-cyclohexanol) according to the initial guaiacol conversion routes via either the **$\mathbf{C^2—OC^7}$** or **H-addition** that form these products. The turnover rates for the **$\mathbf{C^2—OC^7}$** ($r_{C^2-OC^7}$) and **H-addition** ($r_{\mathrm{H-addition}}$) routes relate to these site-time-yields according to

$$r_{C^2-OC^7}\left(\frac{\mathrm{mol}_{C_6H_4(OH)(OCH_3)}}{\mathrm{mol}_{\mathrm{Ru,surf}}\cdot \mathrm{h}}\right) = STY_{\mathrm{phenol}} + STY_{\mathrm{cyclohexanone}} + STY_{\mathrm{cyclohexanol}} + STY_{\mathrm{cyclohexane}} \tag{1a}$$

$$r_{\mathrm{H-addition}}\left(\frac{\mathrm{mol}_{C_6H_4(OH)(OCH_3)}}{\mathrm{mol}_{\mathrm{Ru,surf}}\cdot \mathrm{h}}\right) = STY_{\mathrm{2-methoxy-cyclohexanol}} \tag{1b}$$

In the following section, we probe how these rates, $r_{C^2-OC^7}$ and $r_{\mathrm{H-addition}}$, vary with guaiacol concentrations and H_2 pressures.

3.2. Rate dependencies of $C^2—OC^7$ and H-addition during guaiacol and H_2 reactions at water-Ru cluster interfaces

Guaiacol-H_2 reactions were carried out in a semi-batch, gradientless stirred tank reactor, where the H_2 pressure was kept constant (<±0.1 bar). As reactions proceed, only the guaiacol concentration varied with reaction time *t* and its time-dependent concentration is denoted as $C_{C_6H_4(OH)(OCH_3)}(t)$. The turnover rates for **Routes $\mathbf{C^2—OC^7}$** ($r_{C^2-OC^7}$) and **H-addition** ($r_{\mathrm{H-addition}}$) vary with guaiacol concentration and H_2 pressure according to

$$r_j = k_{\mathrm{eff},\,j}\cdot\left[C_{C_6H_4(OH)(OCH_3)}(t)\right]^{\alpha\,j}\cdot\left(P_{H_2}\right)^{\beta\,j} \tag{2}$$

where $k_{\mathrm{eff},\,j}$ is the effective rate constant; α_j and β_j are the effective reaction orders with respect to guaiacol and H_2, respectively, for **Route *j*** (*j* = $C^2—OC^7$ or H-addition). The general governing equation for the total product concentration via **Route *j*** (*j* = $C^2—OC^7$ or H-addition), $C_j(t)$, for this semi-batch reactor at any reaction clock-time is (derivation in Section S1 of Supporting Information)

$$\begin{aligned}\frac{d[C_j(t)]}{dt} &= S_{\mathrm{Ru,surf}}\cdot r_j \\ &= S_{\mathrm{Ru,surf}}\cdot k_{\mathrm{eff},\,j}\cdot\left[C_{C_6H_4(OH)(OCH_3)}(t)\right]^{\alpha\,j}\cdot\left(P_{H_2}\right)^{\beta\,j}\end{aligned} \tag{3a}$$

where $S_{\mathrm{Ru,surf}}$ denotes the number of exposed Ru sites per liquid volume. The Ru site density remained unchanged throughout the reaction, confirmed from identical product concentration profiles, obtained at two different Ru catalyst amounts, when plotting them as a function of the product of reaction clock time and catalyst amount (similar to variable time normalization analysis [27], in Section S2 of Supporting Information). Eq. (3a), upon rearranging and integrating, gives

$$\begin{aligned}C_j(t) &= S_{\mathrm{Ru,surf}}\cdot\int_0^t r_j\,dt = S_{\mathrm{Ru,surf}}\cdot k_{\mathrm{eff},\,j}\cdot\left(P_{H_2}\right)^{\beta\,j} \\ &\quad\cdot\int_0^t\left[C_{C_6H_4(OH)(OCH_3)}(t)\right]^{\alpha\,j}dt\end{aligned} \tag{3b}$$

Substituting Eqs. (1a) and (1b) into Eq. (3b) gives

$$\begin{aligned}C_{C^2-OC^7}(t) &= C_{\mathrm{phenol}}(t) + C_{\mathrm{cyclohexanone}}(t) + C_{\mathrm{cyclohexanol}}(t) \\ &\quad + C_{\mathrm{cyclohexane}}(t)\end{aligned} \tag{3c}$$

and

$$C_{\mathrm{H-addition}}(t) = C_{\mathrm{2-methoxy-cyclohexanol}}(t) \tag{3d}$$

We note that $C_j(t)$ is linearly proportional to the yield of the specific route of either **$\mathbf{C^2—OC^7}$** or **H-addition**.

Fig. 1a shows the total product concentrations for **Route $\mathbf{C^2—OC^7}$** versus **Route H-addition** at any instantaneous clock time, $C_{C^2-OC^7}(t)$ vs. $C_{\mathrm{H-addition}}(t)$, for a series of experiments with varying initial guaiacol concentration (9.1×10^{-3}–9.3×10^{-2} M) at 423 K and 30 bar H_2. These $C_j(t)$ values remain proportional to each other, irrespective of the initial guaiacol concentrations and conversion levels. Fig. 1b shows these values for a constant initial guaiacol concentration but at different H_2 pressures (10–55 bar). For each H_2 pressure, $C_{C^2-OC^7}(t)$ remains proportional to $C_{\mathrm{H-addition}}(t)$. These strict linear relations between $C_{C^2-OC^7}(t)$ and $C_{\mathrm{H-addition}}(t)$ further confirm that the **$\mathbf{C^2—OC^7}$ cleavage** and **H-addition** routes are truly independent from each other; in other words, the products from both routes do not interconvert. As H_2 pressure increases, the slopes of these linear correlations decrease monotonically, an indication that the selectivity towards **Route $\mathbf{C^2—OC^7}$** decreases with increasing H_2 pressure. In contrast, the slopes and the related selectivity do not vary with guaiacol concentration, irrespective of the extent of reaction, as shown from these strict linear relations in Fig. 1a and b. For each H_2 pressure, these slopes, $\gamma(P_{H_2})$, reflect the $C_{C^2-OC^7}(t)$-to-$C_{\mathrm{H-addition}}(t)$ ratios and acquire the following expression, as derived from expanding the $C_{C^2-OC^7}(t)$-to-$C_{\mathrm{H-addition}}(t)$ ratios with Eq. (3b):

$$\begin{aligned}\gamma(P_{H_2}) &= \frac{C_{C^2-OC^7}(t)}{C_{\mathrm{H-addition}}(t)} \\ &= \frac{k_{\mathrm{eff},\,C^2-OC^7}}{k_{\mathrm{eff,\,H-addition}}}\cdot\left(P_{H_2}\right)^{\beta_{C^2-OC^7}-\beta_{\mathrm{H-addition}}} \\ &\quad\cdot\int_0^t\left[C_{C_6H_4(OH)(OCH_3)}(t)\right]^{\alpha_{C^2-OC^7}-\alpha_{\mathrm{H-addition}}}dt\end{aligned} \tag{4}$$

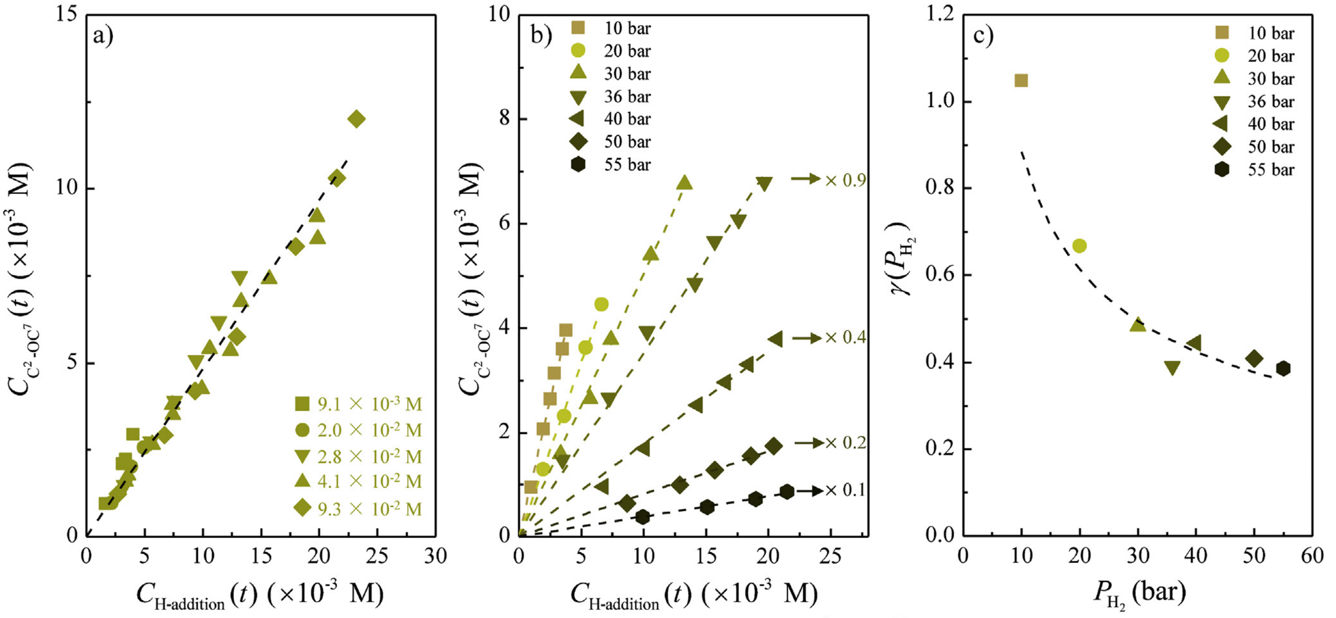

Fig. 1. Sum of the products' concentration formed via **Route C^2-OC^7** [$C_{C^2\text{ - }OC^7}(t)$] as a function of that of the product formed via **Route H-addition** [$C_{\text{H - addition}}(t)$] at (a) initial guaiacol concentrations of 9.1 × 10^{-3} M to 9.3 × 10^{-2} M and 30 bar H_2 (dash line from linear regression) and (b) initial guaiacol concentration of 4.0 (±0.2) × 10^{-2} M and 10–55 bar H_2 (dash lines from linear regressions); (c) Parameter $\gamma(P_{H_2})$ (Eq. (5)), derived from slopes of linear relations in Fig. 1a and b, plotted as a function of P_{H_2} (dash line from non-linear regression by using Eq. (5) as the objective function) during guaiacol-H_2 reactions (9.1 × 10^{-3} M to 9.3 × 10^{-2} M guaiacol and 10–55 bar H_2) on 1 wt% Ru/C (14 nm of cluster size) in the aqueous phase at 423 K.

As shown in Fig. 1a and b, $\gamma(P_{H_2})$ remains insensitive to both the guaiacol concentration [$C_{C_6H_4(OH)(OCH_3)}(t)$] and t, for each H_2 pressure. Such insensitivities could occur only when the effective reaction orders towards guaiacol are identical for both of the routes ($\alpha_{C^2\text{ - }OC^7} = \alpha_{\text{H - addition}}$). In this case, Eq. (4) simplifies to

$$\gamma(P_{H_2}) = \frac{C_{C^2\text{ - }OC^7}(t)}{C_{\text{H - addition}}(t)} = \frac{k_{\text{eff, }C^2\text{ - }OC^7} \cdot (P_{H_2})^{\beta_{C^2\text{ - }OC^7}}}{k_{\text{eff, H - addition}} \cdot (P_{H_2})^{\beta_{\text{H - addition}}}} \tag{5}$$

where $\gamma(P_{H_2})$ is a single-valued function of H_2 pressure (P_{H_2}). Fig. 1c shows that the $\gamma(P_{H_2})$ values, determined from the slopes in Fig. 1a and b, decrease with increasing P_{H_2}. A non-linear regression of this $\gamma(P_{H_2})$ and P_{H_2} relation against Equation (5) as the objective function leads to a rate constant ratio for C^2—OC^7 cleavage to H-addition [$k_{\text{eff, }C^2\text{ - }OC^7} \cdot (k_{\text{eff, H - addition}})^{-1}$] of 3.0 ± 0.5 and a difference in the effective H_2 order between the two routes [$\beta_{C^2\text{ - }OC^7} - \beta_{\text{H - addition}}$] of −0.5 ± 0.0, as summarized in Table 2.

Although the effective reaction orders to guaiacol for both routes are identical ($\alpha_{C^2\text{ - }OC^7} = \alpha_{\text{H - addition}}$), their exact values have yet to be determined. The total product concentrations $C_{C^2\text{-}OC^7}(t)$ and $C_{\text{H - addition}}(t)$ vary with the initial guaiacol concentration, $C_{C_6H_4(OH)(OCH_3)}(0)$, and reaction time according to the integration of the rate expression in Eq. (3a) to reaction time t at a constant α_j value. The following relation derived from solving Eq. (3a) analytically by integration, after substituting Eq. (5) into Eq. (3a), according to the derivation in Section S1 of Supporting Information

$$\frac{\left[C_{C_6H_4(OH)(OCH_3)}(0)\right]^{1-\alpha\ j} - \left[C_{C_6H_4(OH)(OCH_3)}(0) - \sum_j C_j(t)\right]^{1-\alpha_j}}{(1-\alpha_j)\cdot\left[1+\gamma(P_{H_2})\right]} = S_{\text{Ru,surf}} \cdot k_{\text{eff, H - addition}} \cdot (P_{H_2})^{\beta\ \text{H - addition}} \cdot t \tag{6}$$

where $\sum_j C\ _j(t)$ denotes the product concentration sum via **Route *j*** (j = C^2—OC^7 or H-addition). At a given H_2 pressure, terms $C_{C_6H_4(OH)(OCH_3)}(0)$, $S_{\text{Ru,surf}}$, P_{H_2}, and $k_{\text{eff, H - addition}} \cdot (P_{H_2})^{\beta\ \text{H - addition}}$ in Eq. (6) are constants; terms $\sum_j C\ _j(t)$ [sum of $C_{C^2-OC^7}(t)$ and $C_{\text{H - addition}}(t)$], t, and $\gamma(P_{H_2})$ values are measurable. This leaves α_j as the only unknown. This treatment resembles the kinetic analysis method previously developed for obtaining the reaction order numerically for a homogeneous catalytic reaction that selectively produces one product in a batch reactor (i.e., variable time normalization analysis [27]). We, however, take the analysis further by applying the method to treat this multiphase heterogeneous catalytic system with gas, liquid, and solid phases and multiple, concomitant pathways. We also derive from such analysis the

Table 2
Rate parameters determined from non-linear regressions of rate data (in Figs. 1 and 2) during aqueous phase guaiacol-H_2 reactions on dispersed Ru clusters at 423 K (9.1 × 10^{-3} M to 9.3 × 10^{-2} M guaiacol, 10–55 bar H_2, 1 wt% Ru/C, 14 nm mean Ru cluster diameter) with the proposed rate equations (Eqs. (2), (5), (6), and (7b)).

Parameters	$\frac{k_{\text{eff, }C^2\text{ - }OC^7}}{k_{\text{eff, H - addition}}}$ [a]	$\beta_{C^2\text{ - }OC^7} - \beta_{\text{H - addition}}$ [a]	α_j [b]	$k_{\text{eff,H - addition}}$ [c]	$k_{\text{eff,}C^2\text{ - }OC^7}$ [d]	$\beta_{\text{H - addition}}$ [c]	$\beta_{C^2\text{ - }OC^7}$ [d]
Unit	–	–	–	$\frac{(\text{mol}_{C_6H_4(OH)(OCH_3)})^{0.78}\cdot L^{0.22}}{\text{mol}_{\text{Ru,surf}}\cdot h\cdot \text{bar}^{1.46}}$	$\frac{(\text{mol}_{C_6H_4(OH)(OCH_3)})^{0.78}\cdot L^{0.22}}{\text{mol}_{\text{Ru,surf}}\cdot h\cdot \text{bar}^{0.93}}$	–	–
Values	3.0 ± 0.5	−0.5 ± 0.0	0.22 ± 0.02	98 ± 15	291 ± 91	1.46 ± 0.04	0.93 ± 0.09

[a] Non-linear regression of results in Fig. 1 by using Eq. (5) and an objective function.
[b] Non-linear regression of concentrations in Fig. 1a and b by using Eq. (6) and an objective function.
[c] Non-linear regressions of results in Fig. 2a, b, and c.
[d] Non-linear regression of results in Figs. 1 and 2 by using Eqs. (5) and (7b) and objective functions.

analytical solution in Eq. (6), which upon non-linear regression against the rate data in Fig. 1 provides the effective reaction orders with respect to guaiacol for both routes, $\alpha_{C^2\text{ - }OC^7}$ and $\alpha_{H\text{ - addition}}$, of 0.22 ± 0.02 at 30 bar H_2.

From Eq. (2), the standard guaiacol turnover numbers $[\eta(P_{H_2},t)]$ via **Route H-addition** at any H_2 pressure and reaction clock time, when carrying out such reaction in a hypothetical, continuous stirrer tank reactor (CSTR) to maintain the guaiacol concentration at the standard concentration of 1 M (C^o) and H_2 pressure to be P_{H_2} throughout the entire reaction time, is

$$\begin{aligned}\eta(P_{H_2},t) &= \int_0^t (r_{H\text{ - addition}})dt \\ &= \int_0^t \left[k_{\text{eff, H - addition}} \cdot [C^o]^{\alpha\text{ H - addition}} \cdot (P_{H_2})^{\beta\text{ H - addition}}\right]dt \\ &= k_{\text{eff, H - addition}} \cdot (P_{H_2})^{\beta\text{ H - addition}} \cdot t \cdot [C^o]^{\alpha_{\text{H - addition}}} \end{aligned} \tag{7a}$$

Dividing both side of the Eq. (6) by $S_{\text{Ru,surf}}$ and substituting the resulting expression of $k_{\text{eff, H - addition}} \cdot (P_{H_2})^{\beta\text{ H - addition}} \cdot t$ and the guaiacol reaction orders ($\alpha_{C^2\text{ - }OC^7} = \alpha_{H\text{ - addition}} = 0.22 \pm 0.02$) into Eq. (7a) lead to

$$\begin{aligned}\eta(P_{H_2},t) &= k_{\text{eff, H - addition}} \cdot (P_{H_2})^{\beta\text{ H - addition}} \cdot t \cdot [C^o]^{0.22} \\ &= \frac{[C_{C_6H_4(OH)(OCH_3)}(0)]^{0.78} - \left[C_{C_6H_4(OH)(OCH_3)}(0) - \sum_j C_j(t)\right]^{0.78}}{(1-\alpha_j)\cdot[1+\gamma(P_{H_2})]\cdot S_{\text{Ru,surf}}} \\ &\quad \cdot [C^o]^{0.22} \end{aligned} \tag{7b}$$

Fig. 2a shows the guaiacol turnover number, $\eta(P_{H_2},t)$, at 30 bar H_2 and various initial guaiacol concentrations ($C_{C_6H_4(OH)(OCH_3)}(0)$ = 9.1×10^{-3} to 9.3×10^{-2} M) as a function of reaction time t; Fig. 2b shows similar trends for $\eta(P_{H_2},t)$ values, but for different H_2 pressures (10–55 bar), while keeping the initial guaiacol concentration constant at 4.0 ± 0.2 × 10^{-2} M. These $\eta(P_{H_2},t)$ values increase linearly with reaction time t, as predicted from Eq. (7b). These strict linear relations, irrespective of the initial guaiacol concentration and the operating H_2 pressure, confirm that the reaction orders to guaiacol for both routes, $\alpha_{C^2\text{ - }OC^7}$ and $\alpha_{H\text{ - addition}}$, are indeed constant and remain at 0.22 over a wide range of H_2-guaiacol molar ratio, spanning from 26 to 1133. From Eq. (7b), the slopes from these linear relations between $\eta(P_{H_2},t)$ and t equal $k_{\text{eff, H - addition}} \cdot (P_{H_2})^{\beta_{\text{H - addition}}}$: the product of $k_{\text{eff, H - addition}}$, the effective rate constant, and $(P_{H_2})^{\beta_{\text{H - addition}}}$ (i.e., the H_2 dependency term) for **Route H-addition**. Fig. 2c plots these $k_{\text{eff, H - addition}} \cdot (P_{H_2})^{\beta_{\text{H - addition}}}$ values as a function of H_2 pressure, and a non-linear regression of these data gives $k_{\text{eff, H-addition}}$, the rate constant, of 98 ± 15 $(\text{mol}_{C_6H_4(OH)(OCH_3)})^{0.78} \cdot L^{0.22} \cdot (\text{mol}_{\text{Ru,surf}} \cdot h \cdot \text{bar}^{1.46})^{-1}$ and $\beta_{\text{H-addition}}$, the effective H_2 dependence, of 1.46 ± 0.04 for **Route H-addition**. These rate parameter values, taken together with the rate constant ratio $[k_{\text{eff, }C^2\text{ - }OC^7} \cdot (k_{\text{eff, H - addition}})^{-1}]$ of 3.0 ± 0.5 (Table 2) and effective H_2 order differences ($\beta_{C^2\text{ - }OC^7} - \beta_{\text{H - addition}}$) of –0.5 ± 0.0 (Table 2), give $k_{\text{eff, }C^2\text{ - }OC^7}$ of 291 ± 91 $(\text{mol}_{C_6H_4(OH)(OCH_3)})^{0.78} \cdot L^{0.22} \cdot (\text{mol}_{\text{Ru,surf}} \cdot h \cdot \text{bar}^{0.93})^{-1}$ and $\beta_{C^2\text{ - }OC^7}$ of 0.93 ± 0.09. Table 2 summarizes these $k_{\text{eff, }j}$, α_j, and β_j values for both routes. These parameter values, when substitute into Eqs. (4) and (6), give the predicted product concentrations $C_{C^2\text{-}OC^7}(t)$ and $C_{\text{H - addition}}(t)$, as also included as dotted lines in Fig. 3a and b, respectively, for a direct comparison to the measured data. Fig. 3a and b provide the parity plots of these predicted versus measured concentrations for **Routes C²—OC⁷** and **H-addition**, respectively. Perturbation analyses in Section S3 of Supporting Information show that Parameters β_j and $k_{\text{eff, H-addition}}$ are highly sensitive to local variations. For example, a change in their values by ±10% would cause a change in the sum of the squares of residuals by more than 68%. In contrast, Parameters α_j and $k_{\text{eff, }C^2\text{ - }OC^7}$ are much less sensitive to local variations-a change of ±10% would lead to a commensurate change of the sum of the squares of residuals by more than 16%. This is expected, because (i) the effective guaiacol orders are close to zero (α_j = 0.22 ± 0.02), thus a change in their values by ±10% would not cause significant changes in the predicted $C_{C^2\text{-}OC^7}(t)$ and $C_{\text{H - addition}}(t)$ values, and

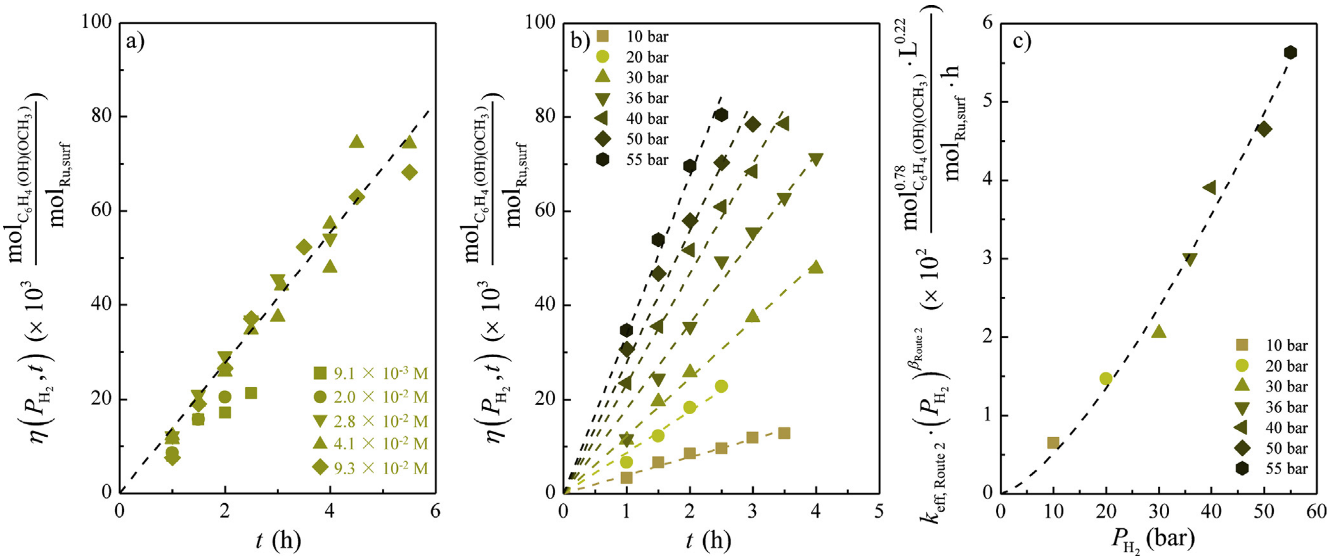

Fig. 2. Parameter $\eta(P_{H_2},t)$ (Eq. (7b)) plotted against reaction time t at a) initial guaiacol concentrations of 9.1×10^{-3} M to 9.3×10^{-2} M and 30 bar H_2 (dash line from linear regression) and b) initial guaiacol concentration of 4.0 (±0.2) × 10^{-2} M and 10–55 bar H_2 (dash lines from linear regressions); c) term $k_{\text{eff, H - addition}} \cdot (P_{H_2})^{\beta_{\text{H - addition}}}$, derived from the slopes of linear relations in Fig. 2a and b, plotted as a function of P_{H_2} (dash line from non-linear regression) during guaiacol-H_2 reactions (9.1×10^{-3} M to 9.3×10^{-2} M guaiacol and 10–55 bar H_2) on 1 wt% Ru/C (14 nm of cluster size) in the aqueous phase at 423 K.

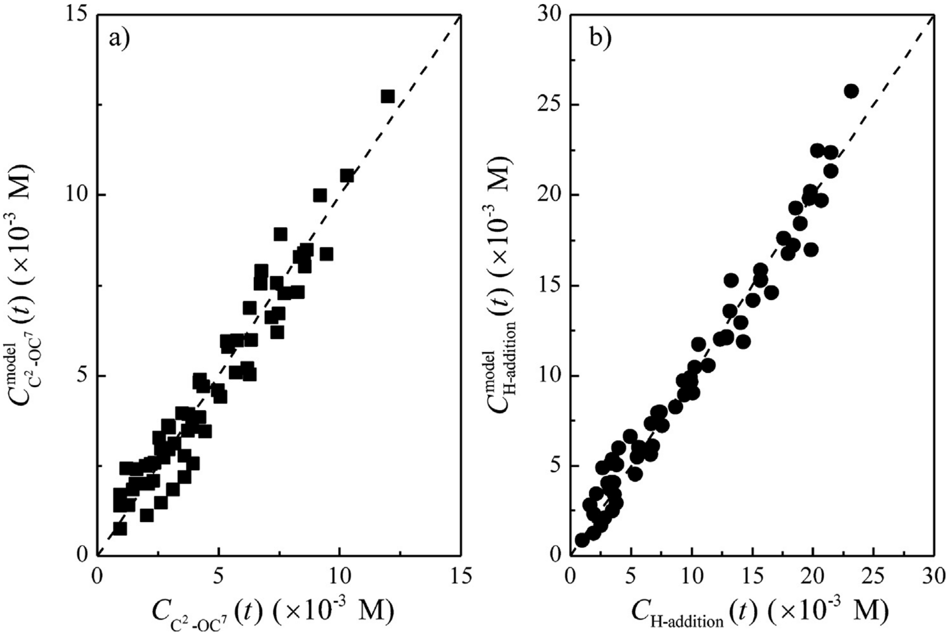

Fig. 3. Parity plots for the (a) sum of the products' concentration formed via **Route C^2—OC^7** [$C_{C^2-OC^7}(t)$] and (b) sum of the product concentration formed via **Route H-addition** [$C_{H-addition}(t)$] during guaiacol-H_2 reactions (9.1×10^{-3} M to 9.3×10^{-2} M guaiacol and 10–55 bar H_2) on 1 wt% Ru/C (14 nm of cluster size) in the aqueous phase at 423 K.

(ii) the selectivities towards **Route C^2—OC^7** are much smaller than **Route H-addition**, thus the regressed $k_{eff,\,C^2-OC^7}$ value remain small and insensitive to its perturbation.

The effective reaction orders α_j and β_j in Table 2 are direct consequences of the surface elementary steps, their reversibility, their kinetic relevance, and the identity of the most abundant surface intermediates. The low reaction order towards guaiacol ($\alpha_j = 0.22 \pm 0.02$) indicates that guaiacol-derived species must occupy most of the Ru sites. On such surfaces, effective H_2 dependence of **Route C^2—OC^7**, $\beta_{C^2-OC^7}$, is near unity (0.93 ± 0.09) and smaller than that of **Route H-addition** ($\beta_{H-addition} = 1.46 \pm 0.04$) by 0.5. The positive H_2 dependence for both routes suggests that guaiacol activation requires the addition of one or more H-adatom (H^*), which is formed via H_2 dissociative adsorption. For each H^* addition step, it would cause the rate expression to acquire a 0.5 order dependence on H_2 pressure, as term $(P_{H_2})^{0.5}$ presents in the numerator of the rate expression [23]. Since $\beta_{C^2-OC^7}$ is smaller than $\beta_{H-addition}$ by 0.5, this indicates that the guaiacol turnovers via **Route C^2—OC^7** require one less H^* than that via **Route H-addition**.

3.3. Elementary steps of *C^2—OC^7 cleavage* and *H-addition* during guaiacol and H_2 reaction at water-Ru cluster interfaces

We propose a mechanistic framework for guaiacol-H_2 catalytic sojourns at the water and Ru interfaces, consistent with the effective dependencies α_j and β_j (Table 2), rate data (Figs. 1 and 2), carbon selectivities (Table 1 and Fig. 1), relative reactivities of intermediates and products (Table 1), and overall reaction network (Scheme 1). We then probe and confirm the reversibility of H^* addition step via H-D isotopic exchange studies with guaiacol-H_2-D_2O mixtures in Section 3.4. The proposed framework remains consistent also with H-D isotopic exchange results of aromatic compounds (e.g., benzene [28] and phenol [29]), adsorption configurations of aromatics on Ru(0 0 0 1) surfaces with HREELS [30], TPD [30], and LEED [30–32] studies under ultra-high vacuum, and reaction energies derived from DFT calculations on Ru (0 0 0 1) surfaces under ultra-high vacuum [20,21].

Scheme 2 shows the proposed mechanistic framework. H_2 dissociatively adsorbs as two H-adatoms (denoted as H^*, Step 1). H_2O molecule from the solvent adsorbs either molecularly as H_2O^* (Step 2) or dissociatively as H^* and OH^* (Step 3) [21,23]. Each H^*, H_2O^*, or OH^* intermediate occupies a Ru site. In contrast, guaiacol adsorbs on an ensemble of Ru sites. Previous studies have established that benzene, the parental structure of guaiacol, occupies three Ru surface atoms and adsorbs in parallel to Ru(0 0 0 1) surfaces, irrespective of its surface coverage, as shown from: (i) high resolution electron energy loss spectroscopy (HREELS) experiments, which show insignificant dynamic dipole moment perpendicular to the surface and the absence of dipole moment enhancement of the in-plane modes, especially C-H vibrational stretching ($\nu_{C\text{-}H}$), over all benzene coverages [30]; (ii) LEED patterns, which correspond to benzene predominantly occupying three Ru sites at all coverages [30–32]; (iii) DFT calculations on Ru(0 0 0 1) surfaces under ultra-high vacuum, which give benzene adsorption in planar configurations on three Ru sites as the most stable species [21]. Comparing to benzene, the adsorption of guaiacol and guaiacol-derived species require additional Ru site(s), because of their additional hydroxyl and methoxy substituents. In fact, DFT calculations suggest that guaiacol-derived aromatic intermediates occupy approximately four Ru ensemble sites on Ru(0 0 0 1) surfaces at all coverages [21]. For the molecular guaiacol adsorption, C^2, C^4, C^6, and hydroxyl oxygen atom of guaiacol directly bind atop of four Ru atoms, whereas the oxygen atom of methoxy group resides closer to the hcp hollow site and becomes tilted away from Ru surfaces under ultra-high vacuum [21]. In fact, *Ab Initio* Molecular Dynamic (AIMD) simulations have shown that guaiacol adsorbs in parallel to Ru (0 0 0 1) surfaces on approximately four Ru ensemble sites at high guaiacol surface coverages (0.083 ML), in the presence of water layers at 423 K [33]. These surface science studies, DFT calculations, and AIMD simulations led us to propose that an adsorbed guaiacol, denoted here as $C_6H_4(OH)(OCH_3)$-χ^*, occupies an ensemble of Ru sites with χ number of Ru atoms ($\chi > 3$).

$C_6H_4(OH)(OCH_3)$-χ^* intermediates undergo a series of H^* addition events onto their benzylic ring, which break their aromaticity. Some of these H^* addition events must be reversible, as demonstrated previously from: (i) the detection of D-H exchanged

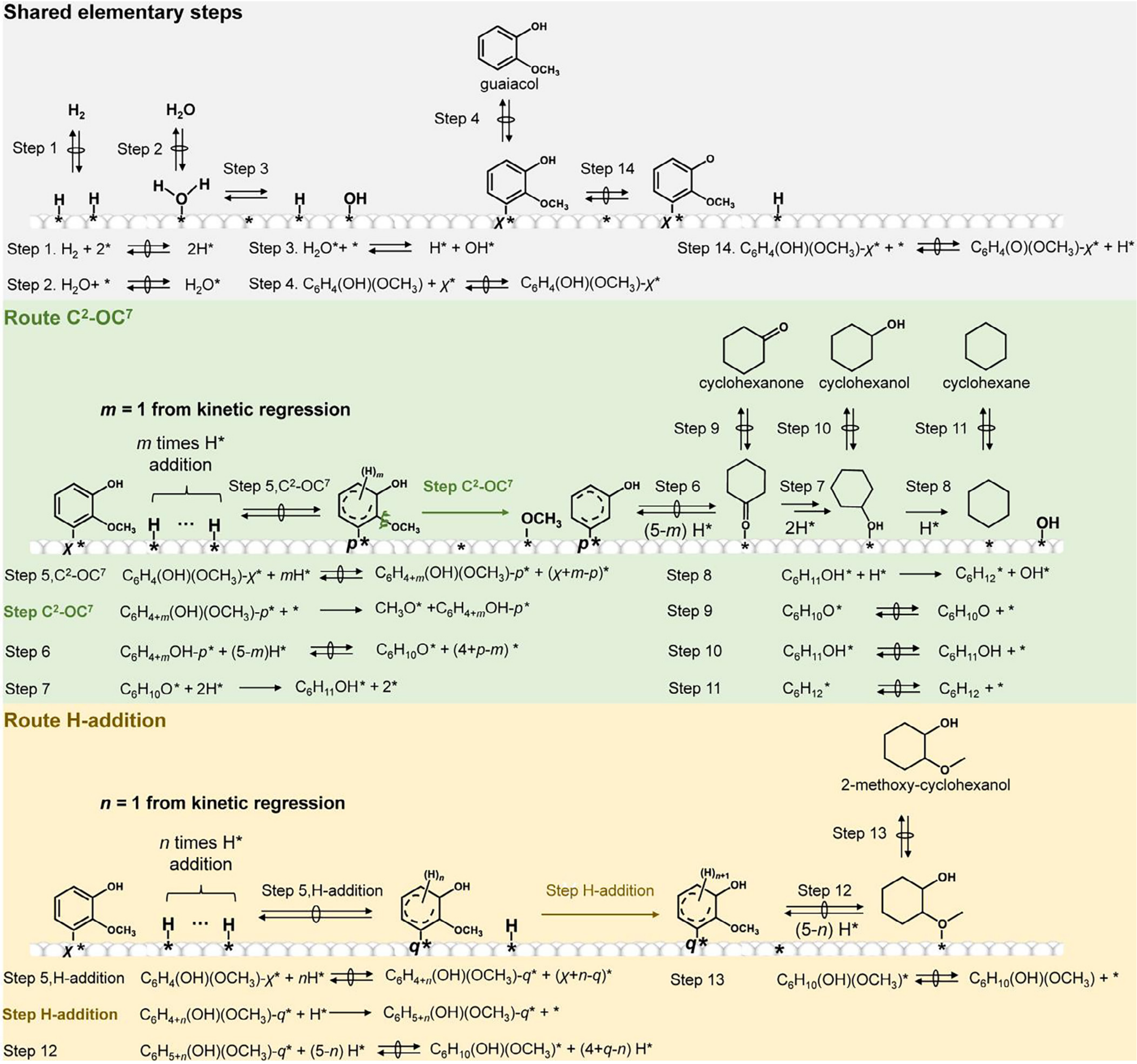

Scheme 2. A proposed sequence of elementary steps for guaiacol-H_2 reactions in the aqueous phase on Ru clusters. (* refers to a Ru surface site, -l^* denotes l number of Ru sites in a surface ensemble ($l = \chi$, p, or q); $\longrightarrow$, $\rightleftarrows$, $\dashrightarrow$, and $\overset{\circ}{\rightleftarrows}$ denote an irreversible step, a reversible step, lumped, irreversible H-addition steps, and a quasi-equilibrated step, respectively).

benzene ($C_6D_{6-x}H_x$, $x = 1–6$) from the surface reactions between H^* and adsorbed, deuterated benzene (C_6D_6) on Ru(0 0 0 1) surfaces in temperature programmed desorption-mass spectrometry (TPD-MS) experiments [28], and (ii) the formation of $C_6D_{5-x}H_xOH$ ($x = 1–5$) from deuterated phenol (C_6D_5OD) and H_2 reactions in D_2O on 5 nm Ru clusters supported on TiO_2 at 573 K [29]. Under ultra-high vacuum, previous DFT calculations on uncovered Pt (1 1 1) have shown that the adsorbed phenol undergoes four H^* addition steps [34] and for p-cresol, which is basically a phenol with an additional methyl group, three of the steps [35], forming a partially hydrogenated phenolic intermediate prior to their respective kinetically relevant C—OH bond cleavage reaction [34,35].

DFT studies have shown that the sequential H-addition and ring saturation events on aromatic species progressively decrease the size of the metal ensemble required for the adsorption of partially hydrogenated benzylic intermediates: (i) on Ru(0 0 0 1) surface, m-cresol adsorbs on ~five Ru sites, whereas the hydrogenated product, 3-methylcyclohexanone, adsorbs on ~ two Ru sites [36]; (ii) on Pt(1 1 1) surface, phenol (C_6H_5OH) adsorbs on four vacant Pt sites, whereas its progressively hydrogenated species C_6H_7OH, C_6H_9OH, and $C_6H_{11}OH$ (cyclohexanol) adsorb on three, two, and one vacant Pt site(s), respectively [37]; (iii) On Pt(1 1 1) surface that are either uncovered or partially covered with H-adatoms, benzene, the parental structure of phenol, when hydrogenates, also decrease its ensemble site requirements from about three vacant Pt sites to one vacant Pt site [38].

H-D isotopic exchange studies with benzene [28] and phenol [29], DFT studies on m-cresol [36], phenol [37], and benzene [38], and the measured effective H_2 dependences that are larger than 0.5, taken together, suggest that $C_6H_4(OH)(OCH_3)$-χ^* undergoes a series of quasi-equilibrated H^* addition events to form partially hydrogenated guaiacol intermediates, as shown in Steps 5, C^2—OC^7 and 5, H-addition of Scheme 2. In each of these H* addition events, an H-adatom adds to an aromatic carbon atom (one of the carbons in C^1—C^6), forming C—H bond and thus increasing the degree of ring-saturation. The number of Ru sites required to accommodate the partially hydrogenated guaiacol intermediates ranges from 1 to χ ($\chi > 3$) and decreases as the reaction proceeds further along the reaction coordinate, as the benzylic ring becomes increasingly saturated. Quasi-equilibrium assumptions require that these intermediates to be treated as a chemical lump, before the sequential, kinetically relevant step that either cleaves their C^2—OC^7 bond or accepts H-adatoms in **Routes C^2—OC^7** or **H-addition**, respectively.

For **Route C^2—OC^7**, $C_6H_4(OH)(OCH_3)\text{-}\chi^*$ undergoes m number of quasi-equilibrated H-addition events ($0 \le m \le 6$), forming a reactive $C_6H_{4+m}(OH)(OCH_3)\text{-}p^*$ (p denotes the number of Ru sites required to adsorb the partially hydrogenated species, $1 \le p \le \chi$) intermediate (Step 5, C^2—OC^7) before the sequential, kinetically relevant C^2—OC^7 cleavage (Step C^2—OC^7) that forms a $C_6H_{4+m}(OH)\text{-}p^*$ and surface methoxy (CH_3O^*), as shown in Scheme 2. We rule out the alternate C^2—OC^7 cleavage step that requires an H* (Step C^2—OC^7, II, Section S4 of Supporting Information), because this step is 74 kJ mol^{-1} more endothermic than Step C^2—OC^7 and most likely has a much higher barrier. The $C_6H_{4+m}(OH)\text{-}p^*$ undergoes a series of kinetically irrelevant H* additions, with its C^1—O bond either intact or cleaved, forming an adsorbed cyclohexanone ($C_6H_{10}O^*$, Step 6) and then an adsorbed cyclohexanol ($C_6H_{11}OH^*$, Step 7) or forming an adsorbed cyclohexane ($C_6H^*_{12}$, Step 8), respectively. The desorption of $C_6H_{10}O^*$, $C_6H_{11}OH^*$, and $C_6H^*_{12}$ in Steps 9, 10, and 11, respectively, completes the catalytic cycle for C^2—OC^7 cleavage. Direct cleavage of the C^1—O bond in the partially hydrogenated intermediates does not occur, because methoxycyclohexane remains undetectable during guaiacol-H$_2$ reactions (Table 1, Section 3.1).

For **Route H-addition**, $C_6H_4(OH)(OCH_3)\text{-}\chi^*$ undergoes n number of quasi-equilibrated H* addition events ($0 \le n \le 5$) that form a reactive $C_6H_{4+n}(OH)(OCH_3)\text{-}q^*$ (q denotes the number of Ru sites required to adsorb the partially hydrogenated species, $1 \le q \le \chi$) intermediate (Step 5, H-addition), before its reaction with another H* in a kinetically relevant step to evolve $C_6H_{5+n}(OH)(OCH_3)\text{-}q^*$ (Step H-addition), as shown in Scheme 2. $C_6H_{5+n}(OH)(OCH_3)\text{-}q^*$ then undergoes rapid, kinetically irrelevant hydrogenation, leading to an adsorbed 2-methoxy-cyclohexanol [$C_6H_{10}(OH)(OCH_3)^*$, Step 12], which desorbs as 2-methoxy-cyclohexanol (Step 13), completing the catalytic cycle.

Aside from these catalytic cycles, chemisorbed guaiacol [$C_6H_4(OH)(OCH_3)\text{-}\chi^*$] may also cleave its O—H bond, forming adsorbed, deprotonated guaiacol and H* (Step 14). DFT calculations have shown that this O—H bond cleavage step is exothermic with a small activation barrier (heat of reaction of −77 kJ·mol^{-1} and barrier of 28 kJ·mol^{-1} [21]) on uncovered Ru(0 0 0 1) surfaces under ultra-high vacuum, leading to the formation of adsorbed, deprotonated guaiacol that has the same footprint with chemisorbed guaiacol, occupying about four Ru ensemble sites. We denote the adsorbed, deprotonated guaiacol as $C_6H_4(O)(OCH_3)\text{-}\chi^*$. We speculate that $C_6H_4(O)(OCH_3)\text{-}\chi^*$ is a spectator that adsorbs and titrates Ru sites, because anisole, a comparable molecule without the hydroxyl functional group and thus is unable to deprotonate, turnovers ~3 times faster than guaiacol at similar conditions (Entry 2 vs. Entry 1 of Table 1, Section 3.1).

Pseudo steady-state treatments carried out on all intermediates involved in the catalytic cycles in Scheme 2 result in the following rate expressions for **Routes C^2—OC^7** ($r_{C^2\text{ - }OC^7}$) and **H-addition** ($r_{\text{H - addition}}$, derivation in Section S5 of Supporting Information):

$$r_{C^2\text{ - }OC^7} = k_{C^2\text{ - }OC^7} K_4 K_{5,\ C^2\text{ - }OC^7}\, a_{C_6H_4(OH)(OCH_3)}(t)\left[\left(K_1 f_{H_2}\right)^{0.5}\right]^m \theta_*^{p+1} \tag{8a}$$

$$r_{\text{H - addition}} = k_{\text{H - addition}} K_4 K_{5,\ \text{H - addition}}\, a_{C_6H_4(OH)(OCH_3)}(t)\left[\left(K_1 f_{H_2}\right)^{0.5}\right]^{n+1} \theta_*^{q+1} \tag{8b}$$

$$\text{where } a_{C_6H_4(OH)(OCH_3)}(t) = C_{C_6H_4(OH)(OCH_3)}(t)\cdot\left(C^o\right)^{-1} \tag{8c}$$

$$\text{and } f_{H_2} = P_{H_2}\cdot\left(P^o\right)^{-1} \tag{8d}$$

where k_j, K_x, θ_* denote the intrinsic rate constant of Step j, equilibrium constant of Step x (x = 1, 4, or 5, j), and the fractional coverage of vacant Ru site, respectively, as defined in Scheme 2; P^o denotes the standard pressure; $a_{C_6H_4(OH)(OCH_3)}(t)$ and f_{H_2} denote the activity of guaiacol and fugacity of H$_2$, respectively, assuming that the activity coefficients of guaiacol and H$_2$ equal unity.

Since the effective guaiacol and H$_2$ dependencies remain insensitive to conversions and thus to the concentrations of all products (Section 3.2), the coverages of intermediates formed after the kinetically relevant steps [e.g., $C_6H_{10}O^*$, $C_6H_{11}OH^*$, $C_6H^*_{12}$, and $C_6H_{10}(OH)(OCH_3)^*$] must remain insignificant. Under ultra-high vacuum, DFT calculations have shown that the initial H* additions onto the benzylic ring of adsorbed guaiacol, $C_6H_4(OH)(OCH_3)\text{-}\chi^*$, on uncovered Ru(0 0 0 1) surfaces that form the adsorbed $C_6H_5(OH)(OCH_3)\text{-}\chi^*$ species is endothermic with negligible reaction entropy change (e.g., ΔH = 47 kJ mol^{-1} and ΔS = −1 J mol^{-1} - K^{-1} on C^1 [21]); the coverage ratio of [$C_6H_5(OH)(OCH_3)\text{-}\chi^*$]-to-[$C_6H_4(OH)(OCH_3)\text{-}\chi^*$] is

$$\theta_{C_6H_5(OH)(OCH_3)\text{-}\chi*}\,\theta^{-1}_{C_6H_4(OH)(OCH_3)-\chi*} = K_{\text{initial H}*\text{ - addition}}\left(K_1 f_{H_2}\right)^{0.5} \tag{9}$$

where $\theta_{C_6H_5(OH)(OCH_3)-\chi*}$ and $\theta_{C_6H_4(OH)(OCH_3)-\chi*}$ denote the fractional coverage of $C_6H_5(OH)(OCH_3)\text{-}\chi^*$ and $C_6H_4(OH)(OCH_3)\text{-}\chi^*$, respectively. $K_{\text{initial H}*\text{ - addition}}$ and K_1 denote the equilibrium constants for the initial H* addition onto the benzylic ring of adsorbed guaiacol and for H$_2$ dissociative adsorption, respectively. Literature has reported these $K_{\text{initial H}*\text{ - addition}}$ and K_1 values to be 4.6×10^{-6} and 6.79×10^7, respectively, at vacuum-Ru(0 0 0 1) interface and 473 K, calculated based on energies derived from DFT calculations, statistical thermodynamics, and van't Hoff Equation [21]. Assuming that the reaction enthalpies and entropies do not vary with the temperature, we extrapolate these equilibrium constant values to 423 K and obtain the $K_{\text{initial H}*\text{ - addition}}$ and K_1 values of 1.21×10^{-6} and 4.78×10^9, respectively. Our DFT study shows that explicit H$_2$O solvent layers do not significantly affect the reaction enthalpies of initial H* addition on $C_6H_4(OH)(OCH_3)\text{-}\chi^*$ on Ru(0 0 0 1); for example, the reaction enthalpies for H* addition on C^5 (Scheme 1) of $C_6H_4(OH)(OCH_3)\text{-}\chi^*$ at vacuum-Ru(0 0 0 1) and water-Ru(0 0 0 1) interfaces are 40 kJ mol^{-1} and 36 kJ mol^{-1} respectively, at 0.083 ML [33]. In addition, solvation free energy from water to H$_2$ [39] and surface H-adatom [40] are near zero. These reasons, together with the assumption that water does not alter the entropies of adsorption, lead $K_{\text{initial H}*\text{ - addition}}$ and K_1 values to remain nearly identical for the cases with or without the water solvent. These $K_{\text{initial H}*\text{ - addition}}$ and K_1 values, together with the H$_2$ pressure used for the reactions (≤55 bar at 298 K), lead to a $\theta_{C_6H_5(OH)(OCH_3)-\chi*}$-to-$\theta_{C_6H_4(OH)(OCH_3)-\chi*}$ coverage ratio that ranges from 0.3 (±0.1) to 0.6 (±0.3). Therefore, the coverages of partially hydrogenated guaiacol are smaller than that of molecularly adsorbed guaiacol on Ru surfaces in the aqueous phase.

In terms of the deprotonated guaiacol, the coverage ratio of deprotonated guaiacol to guaiacol on the surfaces, $\theta_{C_6H_4(O)(OCH_3)\text{-}\chi*}\,\theta^{-1}_{C_6H_4(OH)(OCH_3)-\chi*}$ [where $\theta_{C_6H_4(O)(OCH_3)-\chi*}$ denotes the fractional coverage of $C_6H_4(O)(OCH_3)\text{-}\chi^*$], is

$$\theta_{C_6H_4(O)(OCH_3)\text{-}\chi*}\,\theta^{-1}_{C_6H_4(OH)(OCH_3)-\chi*} = \frac{K_{14}}{\left(K_1 f_{H_2}\right)^{0.5}} \tag{10}$$

Literature has estimated K_{14} value, derived from DFT calculations, statistical thermodynamics, and van't Hoff equation, to be 1.43×10^8 at vacuum-Ru(0 0 0 1) interface and 473 K [21]. Assuming that the reaction enthalpy and entropy of Step 14 (Scheme 2) do not vary with temperature as well as the present of water solvent, we extrapolate the equilibrium constant value from 473 to 423 K and obtain a K_{14} value of 1.51×10^9, using a DFT derived reaction enthalpy (-77 kJ·mol^{-1} of Step 14 [21]). The K_1 and K_{14} values, together with the H_2 pressures used for the reactions (10–55 bar at 298 K), lead to $\theta_{C_6H_4(O)(OCH_3)\text{-}\chi*}\theta^{-1}_{C_6H_4(OH)(OCH_3)-\chi*}$ coverage ratios that range from 3 (±2) × 10^3 to 7 (±4) × 10^3. These coverage ratios suggest that the surface coverages of adsorbed guaiacol and partially-hydrogenated guaiacol must be much smaller than those of the adsorbed, deprotonated guaiacol [$C_6H_4(O)(OCH_3)\text{-}\chi^*$] on Ru surfaces in the aqueous phase.

Multi-site Langmuirian adsorption model [41–43] gives the site balance, by assuming that the coverages of guaiacol, partially-hydrogenated guaiacol, and also the intermediates formed after the kinetically relevant steps remain insignificant and all Ru sites are identical, of (derivation in Section S6 of Supporting Information):

$$\theta_* = \frac{1}{\underset{\substack{\uparrow\\ \theta_*\theta_*^{-1}}}{1} + \underset{\substack{\uparrow\\ \theta_{H*}\theta_*^{-1}}}{\left(K_1 f_{H_2}\right)^{0.5}} + \underset{\substack{\uparrow\\ \chi\cdot\theta_{C_6H_4(O)(OCH_3)\text{-}\chi*}\cdot\theta_*^{-1}}}{\chi\cdot\frac{K_{14}K_4 a_{C_6H_4(OH)(OCH_3)}(t)}{\left(K_1 f_{H_2}\right)^{0.5}}\theta_*^{\chi-1}} + \underset{\substack{\uparrow\\ \theta_{H_2O*}\theta_*^{-1}}}{K_2 a_{H_2O}} + \underset{\substack{\uparrow\\ \theta_{OH*}\theta_*^{-1}}}{\frac{K_3K_2a_{H_2O}}{\left(K_1 f_{H_2}\right)^{0.5}}}} \tag{11}$$

where K_x denotes the equilibrium constant of Step x in Scheme 2 (x = 1, 2, 3, 4, or 14), a_{H_2O} the activity of H_2O, and θ_{z*} the fractional coverage of surface species z^* (z^* = H^*, H_2O^*, or OH^*), respectively. Each term in the denominator of Eq. (11) represents the coverage ratio of the surface species z^*-to-vacant Ru site or the coverage ratio of $C_6H_4(O)(OCH_3)\text{-}\chi^*$-to-vacant Ru site, as indicated directly underneath the equation.

At high H_2 pressures (10–55 bar), the coverage ratio of vacant sites to those occupied by H^* ($\theta_*\theta_{H*}^{-1}$) is negligible [23]. Since the effective reaction orders to guaiacol, $\alpha_{C^2\text{ - }OC^7}$ and $\alpha_{H\text{ - addition}}$, are constant and remain at 0.22 for a wide range of H_2-to-guaiacol ratios (from 26 to 1133, Fig. 2), guaiacol derived species must be the most abundant surface intermediates, and those of H^* and OH^* must remain insignificant. H_2O^* coverages also remain small, because they adsorb much more weakly than guaiacol (heat of adsorption of 57 kJ·mol^{-1} vs. 237 kJ·mol^{-1} on uncovered Ru (0 0 0 1) surfaces) [21]. Taking these relative coverages of H^*, OH^*, H_2O^*, and $C_6H_4(O)(OCH_3)\text{-}\chi^*$ into consideration, simplifying Eq. (11) and substituting the simplified Eq. (11) into Eqs. (8a) and (8b) lead to the rate expressions for **Routes C^2—OC^7** ($r_{C^2\text{ - }OC^7}$) and **H-addition** ($r_{H\text{ - addition}}$):

$$r_{C^2\text{ - }OC^7} = k_{C^2\text{ - }OC^7}K_4K_{5,C^2\text{ - }OC^7}K_1^{0.5m}(\chi K_{14}K_4)^{-\frac{p+1}{\chi}}\left[a_{C_6H_4(OH)(OCH_3)}(t)\right]^{1-\frac{p+1}{\chi}}\left(f_{H_2}\right)^{0.5m+\frac{p+1}{2\chi}} \tag{12a}$$

$$r_{H\text{ - addition}} = k_{H\text{ - addition}}K_4K_{5,H\text{ - addition}}K_1^{0.5(n+1)}(\chi K_{14}K_4)^{-\frac{q+1}{\chi}}\left[a_{C_6H_4(OH)(OCH_3)}(t)\right]^{1-\frac{q+1}{\chi}}\left(f_{H_2}\right)^{0.5(n+1)+\frac{q+1}{2\chi}} \tag{12b}$$

Comparing Eqs. (12a) and (12b) with Eq. (2) leads to:

$$k_{\text{eff},C^2\text{ - }OC^7} = k_{C^2\text{ - }OC^7}K_4K_{5,C^2\text{ - }OC^7}K_1^{0.5m}(\chi K_{14}K_4)^{-\frac{p+1}{\chi}}(P^o)^{-\left(0.5m+\frac{p+1}{2\chi}\right)}(C^o)^{\frac{p+1}{\chi}-1} \tag{13a}$$

$$k_{\text{eff},H\text{ - addition}} = k_{H\text{ - addition}}K_4K_{5,H\text{ - addition}}K_1^{0.5(n+1)}(\chi K_{14}K_4)^{-\frac{q+1}{\chi}}(P^o)^{-\left[0.5(n+1)+\frac{p+1}{2\chi}\right]}(C^o)^{\frac{q+1}{\chi}-1} \tag{13b}$$

$$\alpha_j = 1 - \frac{p+1}{\chi} = 1 - \frac{q+1}{\chi} \tag{13c}$$

$$\beta_{C^2\text{ - }OC^7} = 0.5m + \frac{p+1}{2\chi} \tag{13d}$$

$$\beta_{H\text{ - addition}} = 0.5(n+1) + \frac{p+1}{2\chi} \tag{13e}$$

The regressed α_j and β_j values in Table 2 give $(p+1)/\chi$, $(q+1)/\chi$, m, and n of 0.78 ± 0.02, 0.78 ± 0.02, 1.0 ± 0.1, and 1.0 ± 0.2, respectively, as summarized in Table 3. The m and n values are identical and equal to unity, confirming that chemisorbed guaiacol, $C_6H_4(OH)(OCH_3)\text{-}\chi^*$, undergoes one quasi-equilibrated H^* addition to form a common surface intermediate, $C_6H_5(OH)(OCH_3)\text{-}p^*$, prior to the kinetically relevant step of either C^2—OC^7 cleavage (Step C^2—OC^7) or H^* addition (Step H-addition). In what follows, we confirm the reversibility of both the H_2O^* dissociation (Step 3) and initial H^* addition (Step 5, j) steps that occur prior to the two kinetically relevant steps with H-D isotopic exchange studies.

3.4. Reversibility of initial H-adatom addition onto the benzylic ring of guaiacol probed by guaiacol-D_2O-H_2 reactions

Guaiacol [$C_6H_4(OH)(OCH_3)$, 4.3×10^{-2} M]-D_2O-H_2 (30 bar at 298 K) reaction on 10 mg 1 wt% Ru/C (14 nm Ru clusters size) leads to deuterated guaiacol. Electron ionization mass spectrometer analysis of guaiacol gives its parental molecular ion at a mass-to-charge ratio, m/z, of 124. Any increase in this m/z ratio signifies the incorporation of D-atom onto its benzylic ring, hydroxyl group, and/or methyl group. Aside from its parental molecular ion, guaiacol also loses its methyl group upon electron ionization, giving a base ion at 109 m/z [44,45]. The mass-to-charge ratio of 109 + x (where x = 0–5) relative to 109 reflects the extent of D-atom incorporation onto the benzylic ring and hydroxyl group. The intensity ratio of 124 to 109 m/z and of (124 + x) to (109 + x) m/z remains identical to each other (Fig. S3, Section S7 of Supporting Information) irrespective of the extent of deuteration, confirming that the mass of the leaving methoxy group remains identical as —OCH_3. This result confirms that H-D exchange does not occur on the methyl group, but instead on the hydroxyl and benzylic ring.

On phenol, a parental structure of guaiacol, kinetic analyses and ^1H nuclear magnetic spectroscopy (NMR) show that proton catalyzes the H-atom exchange between its hydroxyl group and H_2O readily at 298 K with a second-order exchange rate constant and activation barrier of 1.5×10^7 M^{-1} s^{-1} and 23 kJ mol^{-1}, respectively [46]. Due to the structural similarity, we assume that the rate constant of H-atom exchange between the hydroxyl groups of guaiacol and H_2O is similar to that between the hydroxyl groups of phenol and H_2O. The H-atom exchange rate constant of phenol (298 K), its activation barrier, together with the deuteron concentration calculated from the D_2O self-ionization equilibrium constant of ~7.9×10^{-7} M at 423 K [2], provide an estimated homogeneous H-D exchange rate of 2.8×10^3 mol·h^{-1} for reactions between the H-atom of the hydroxyl group in guaiacol with the D-atom of D_2O at 423 K.

At the reaction temperature (423 K), the estimated homogeneous hydroxyl proton exchange rate is more than six orders of magnitude larger than the guaiacol turnovers on Ru clusters (1.2×10^{-3} mol·h^{-1}, 10 mg 1 wt% Ru/C). In fact, after an hour of homogeneous guaiacol-D_2O reactions (with neither the Ru catalyst nor H_2) at 323 K, ~70% of the $C_6H_4(OH)(OCH_3)$ converts to $C_6H_4(OD)(OCH_3)$. These results suggest that, during guaiacol-D_2O-H_2 reactions at 423 K, the hydroxyl proton of guaiacol exchanges

Table 3
Parameters derived from parameters in Table 2 and Eqs. (13c)–(13e).

Parameters	$\frac{p+1}{\chi}$[a]	$\frac{q+1}{\chi}$[a]	m[b]	n[c]
Values	0.78 ± 0.02	0.78 ± 0.02	1.0 ± 0.1	1.0 ± 0.1

[a] Derived from α_j value (0.22 ± 0.02, Table 2) and Eq. (13c).
[b] Derived from $\beta_{C^2\text{ - }OC^7}$ value (0.93 ± 0.09, Table 2) and Eq. (13d).
[c] Derived from $\beta_{H\text{ - addition}}$ value (1.46 ± 0.04, Table 2) and Eq. (13e).

with the deuteron from D_2O much more readily than the H-D exchange at the benzylic ring. Thus, this step remains kinetically irrelevant.

During $C_6H_4(OH)(OCH_3)$-D_2O-H_2 reactions (4.3×10^{-2} M guaiacol, 30 bar) with the Ru catalyst, H-D isotopic exchange occurs on the benzylic ring, forming $C_6H_{4-y}D_y(OD)(OCH_3)$ ($y = 1$ or 2, ~13% of remaining guaiacol, Table 4). The reaction forms 2-methoxy-cyclohexanol, the product of **Route H-addition**, with all extents of ring deuteration (92.7% of 2-methoxy-cyclohexanol contains D-atom on its carbon ring), ranging from non-deuterated ($H_{10}D_0$) to near complete deuteration (H_1D_9) of its carbon ring, as shown in Fig. 4. In a separate experiment with the identical amount of catalyst (10 mg) and at 423 K, cyclohexanol (1.1×10^{-1} M $C_6H_{11}OH$)-D_2O-H_2 (30 bar H_2) reactions form less than 2% of H-D exchange products on the carbon ring, as $C_6H_{10}DOD$, after one hour; the corresponding to H-D exchange rate constant of cyclohexanol, estimated by the initial H-D exchange turnover rate normalized to the initial concentration, is at least 5 times smaller than that of guaiacol. These results indicate that the sequential ring-deuteration of 2-methoxy-cyclohexanol, after hydrogenation of guaiacol, is negligible, as its concentration remains low during $C_6H_4(OH)(OCH_3)$-D_2O-H_2 reactions (Fig. 4, $<1.1 \times 10^{-2}$ M). The wide deuteration extents of 2-methoxy-cyclohexanol (Fig. 4) must therefore occur during guaiacol hydrogenation and reflect the reversibility of the partially hydrogenated guaiacol intermediates, before their eventual saturation and desorption as 2-methoxy-cyclohexanol. As these intermediates undergo forward catalytic sojourns, they also recombine with D^* adatoms and desorb as deuterated guaiacol. Meanwhile, the forward catalytic steps of these deuterated guaiacol form the deuterated 2-methoxy-cyclohexanol. This condition also requires that both H^* and D-adatom (D^*) co-exist on Ru surfaces with H_2-D_2O co-reactants, consistent with the proposed reversible water dissociation step (Step 3, Scheme 2).

From guaiacol, the formation of a 2-methoxy-cyclohexanol requires six consecutive H^* or D^* addition events (Scheme 2). That being said, the formation of each non-deuterated 2-methoxy-cyclohexanol would require six sequential H^* addition events, without any D^* addition. The relatively large fraction of non-deuterated 2-methoxy-cyclohexanol (~7%, Fig. 4) has further inferred that the H^* coverages must be much larger than the D^* coverages. The molar ratio of non-deuterated to deuterated 2-methoxy-cyclohexanol depends on the (i) H^*-to-D^* coverage ratio, (ii) H-D equilibrium isotope effects (EIEs) of quasi-equilibrated H-addition events (Step 5, H-addition and Step 12), and (iii) H-D kinetic isotope effect (KIE) of Step H-addition. The EIEs of H^* addition are lower than unity {e.g., 0.64 of H^* addition on carbon atom of CO during CO—H_2 reaction on Co(0 0 0 1) surfaces [47]}, as C—D bond has a lower zero-point energy than C—H bond by a difference of ~−4.8 kJ mol^{-1} [48]. These EIEs compensate the normal H-D kinetic isotope effect (KIE) of Step H-addition, which is ~3 at 423 K on Ru clusters [33]. Based on these values, we further assume that the EIEs compensate completely the KIE during these H^* addition events and estimate the relative abundance of H^*-to-D^* from the deuterium distributions in 2-methoxy-cyclohexanol. The molar fraction of non-deuterated 2-methoxy-cyclohexanol (~7%, Fig. 4), overall six H^* or D^* addition events (Scheme 2), and binomial distribution of H-atom and D-atom incorporations in 2-methoxy-cyclohexanol lead to an estimated H^*-to-D^* coverage ratio of ~2.

Table 4
Summary of guaiacol turnover rates via ring deuteration and ***Route j*** ($j = C^2OC^7$ or H-addition) during guaiacol-H_2-D_2O reactions on Ru clusters at 423 K.

Reactant	Solvent	Guaiacol concentration (M)	Gas phase	Gas pressure (bar, at 298 K)	Catalyst (mg)	Guaiacol turnover rates via ring deuteration[a]		Guaiacol turnover rates via route j[a]	
						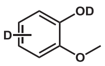	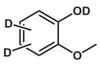	C^2—OC^7	H-addition
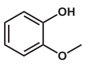	D_2O	4.9×10^{-2}	H_2	30	10	9.7×10^3	8.8×10^2	1.1×10^4	2.4×10^4

[a] Turnover rate has a unit of $mol_{guaiacol} \cdot (mol_{Ru,surf} \cdot h)^{-1}$.

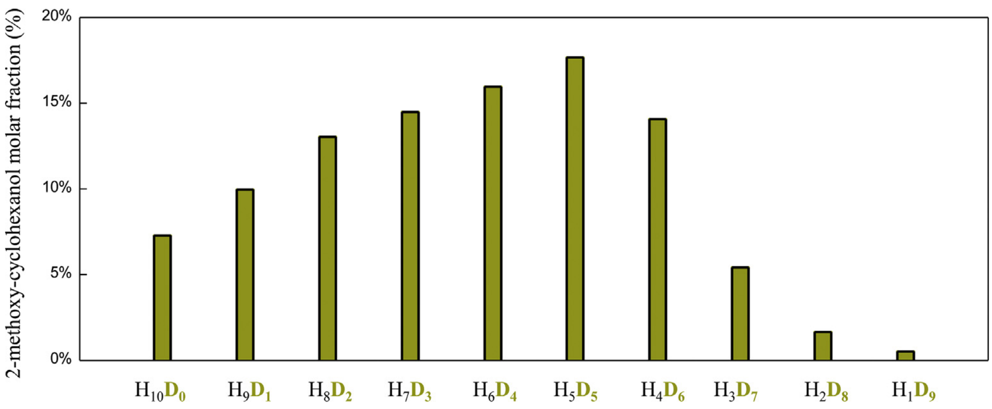

Fig. 4. H-D isotope distributions of H-atoms on the carbon ring of 2-methoxy-cyclohexanol (ten hydrogen atoms in total, derived based on the molecular ion of 2-methoxy-cyclohexanol from mass spectrometer analysis) after one hour of guaiacol (4.3×10^{-2} M guaiacol)-D_2O-H_2 (30 bar) reaction on 10 mg 14 nm 1 wt% Ru/C at 423 K.

This estimated H*-to-D* ratio (~2) is much higher than 0.017, the expected ratio when H_2-D_2O exchange reaction attains chemical equilibrium (derived from the H_2-D_2O initial molar ratio, Section 2.2). Without guaiacol molecules, H_2-D_2O exchange reaches chemical equilibrium much more rapidly at 373 K, a much lower temperature, on the same catalyst [23]. The deviation of H_2-D_2O from equilibrium in the presence of guaiacol, even at a higher temperature (423 K), indicates that deprotonated guaiacol as the most abundant surface intermediate prevents the H_2-D_2O chemical equilibration, because it titrates the available Ru sites (Section 3.3), consistent with the negligible H*, H_2O^*, and OH* coverages concluded in Section 3.3.

Deuterated guaiacol, $C_6H_{4\text{-}y}D_y(OD)(OCH_3)$ (y = 1 or 2), may form from an initiation step that involves either a H-abstraction, before the D* addition on C^b (b = 3, 4, 5, or 6), or vise versa. On aromatic rings, the H-abstraction occurs much more slower than H* addition on transition metal surfaces, as previously established by TPD and HREELS experiments [28], which demonstrate that D-H exchange between H* and deuterated benzene (C_6D_6) occurs prior to its dehydrogenation on Ru(0 0 0 1) [28], and proposed by H-D exchange reactions of phenol-H_2-D_2O and benzene-H_2-D_2O on Ru/TiO_2 (5 nm Ru cluster) at 523 K [29]. At high H_2 pressures (30 bar), we expect that the initial H-abstraction is kinetically formidable and thermodynamically unfavorable; guaiacol deuteration [i.e., $C_6H_{4\text{-}y}D_y(OD)(OCH_3)$ formation] most likely occur via an initial reversible D* addition followed by hydrogen abstraction on C^b, which is consistent with the proposed mechanistic sequence (Scheme 2).

Table 4 compares the guaiacol forward turnover rates via **Route *j*** (j = C^2—OC^7 or H-addition) with those of ring-deuteration, after one-hour $C_6H_4(OH)(OCH_3)$-D_2O-H_2 (4.3 × 10^{-2} M guaiacol, 30 bar H_2) reactions on 1 wt% Ru/C at 423 K. The ring-deuteration rates [i.e., 1.1 × 10^3 $\text{mol}_{\text{guaiacol}}\cdot(\text{mol}_{\text{Ru}}\cdot\text{h}^{-1})$, Table 4] appear to be an order of magnitude smaller than the total forward turnover rates, which include both of the **Routes C^2—OC^7** and **H-addition** [4.4 × 10^4 $\text{mol}_{\text{guaiacol}}\cdot(\text{mol}_{\text{Ru}}\cdot\text{h}^{-1})$, Table 4]. This is because (i) D_2O^* dissociation that forms D* is far away from equilibrium, when Ru surfaces are covered with deprotonated guaiacol, thus fewer D* adatoms are available for the H-D exchange; (ii) only the initial D* (H*-to-D* ratio ~2) addition can lead to deuterated guaiacol, whereas both H* and D* additions lead to **Routes C^2—OC^7** and **H-addition** hydrodeoxygenation products (Step 5, j, Scheme 2). A separate H-D exchange experiment of guaiacol (4.3 × 10^{-2} M guaiacol)-D_2 (1 bar)-D_2O on 14 nm Ru/C shows selective H-D exchange on C^5 of guaiacol, and the D* addition rate is much faster than hydrodeoxygenation rates [33], confirming that Step 5, j is quasi-equilibrated (Scheme 2).

Previous DFT calculations for the initial H* addition on C^1 and C^2 of guaiacol on uncovered Ru(0 0 0 1) surfaces in high vacuum show high barriers (>107 kJ mol^{-1}) and thus conclude that guaiacol hydrodeoxygenation does not initiate via the partial hydrogenation of its aromatic ring but instead via rapid H-abstraction steps from its methyl group (—C^{7}H$_3$) [21]. The calculations, however, do not consider the initial H* addition onto the other carbon atoms within the benzylic ring (i.e., C^3—C^6), which leads to the formation of H-D exchanged guaiacol during $C_6H_4(OH)(OCH_3)$-D_2O-H_2 reactions (Table 4 and Fig. 4). In addition, if the H-abstraction from the methyl group was to occur before the kinetically relevant steps of **Routes C^2—OC^7** and **H-addition**, H-D exchange on the methyl group (-C^{7}H$_3$) would have occur. The H-D exchange on methyl group, however, remains insignificant during the $C_6H_4(OH)(OCH_3)$-D_2O-H_2 reactions (<0.5%) for up to 3.5 h of reaction, which corresponds to an H-D exchange rate on C^7 of much less than 103 $\text{mol}_{\text{guaiacol}}\cdot(\text{mol}_{\text{Ru}}\cdot\text{h}^{-1})$ (Fig. S3, Section S7 of Supporting Information). Based on these H-D isotopic exchange results, we conclude that guaiacol hydrodeoxygenation occurs via an initial hydrogenation on its benzylic ring, as shown in Scheme 2, instead of the direct H-abstraction(s) from its methyl group. In fact, careful H-D isotopic exchange results, together with ^{1}H and ^{13}C NMR studies and first-principle simulations, reveal that the initial H* addition occurs preferentially on C^5, followed by the kinetically relevant H-addition and C^2—OC^7 cleavage steps [33], consistent with the proposed reaction sequence and surface elementary steps in Scheme 2.

4. Conclusion

This study describes the reaction network and elementary reaction sequence during guaiacol and hydrogen reactions at the interface of water-Ru clusters, based on time-dependent kinetic measurements and H-D isotopic assessments in a gradientless semi-batch reactor. On Ru cluster surfaces saturated with deprotonated guaiacol, $C_6H_4(OH)(OCH_3)$—H_2 reactions begin with a quasi-equilibrated H-adatom addition step that forms partially hydrogenated surface intermediate, prior to its sequential reactions of two independent kinetically relevant steps of C^2—OC^7 bond cleavage and H-addition. The former step leads to phenol, cyclohexanone, cyclohexanol, or cyclohexane and the latter to 2-methoxycyclohexanol. Both the C^2—OC^7 bond cleavage and H-addition routes acquire identical, near zero dependence with guaiacol concentration, an indication that these competitive routes proceed via the same guaiacol-derived, partially hydrogenated reactive intermediates on Ru cluster surfaces covered with deprotonated guaiacols as the spectator species. H-D isotopic exchange and effective H_2 dependencies confirm the reversible formation of the common reactive intermediates, as their formation lead to the H-D exchange on the benzylic ring of guaiacol in H_2-D_2O and positive H_2 orders for both C^2—OC^7 bond cleavage and H-addition routes. C^2—OC^7 bond cleavage route, however, exhibits H_2 dependence that is 0.5 order less than that of H-addition route, because the C^2—OC^7 bond cleavage step occurs on a vacant Ru site (*) and requires one less H-adatom (H*) than the competing H-addition step. As a result, the selectivities towards the desired C^2—OC^7 bond cleavage products increase with increasing *-to-H* coverage ratio, which correlates proportionally to the inverse square root of H_2 pressure.

Acknowledgements

This study was supported by Natural Sciences and Engineering Research Council of Canada (NSERC), Valmet, Abellon CleanEnergy, Dupont Canada, Canada Foundation for Innovation (CFI), and Ontario Research Fund-Research Excellence Round 7; J. Shangguan acknowledges Hatch Graduate Scholarship for Sustainable Energy Research. We acknowledge Dr. Joachim Ritter (Dupont) for helpful technical discussions and Dr. Daewoon Jeong for his contribution on the development stage of the experimental work.

Appendix A. Supplementary material

Supplementary data to this article can be found online at https://doi.org/10.1016/j.jcat.2018.11.036.

References

[1] J. He, L. Lu, C. Zhao, D. Mei, J.A. Lercher, Mechanisms of catalytic cleavage of benzyl phenyl ether in aqueous and apolar phases, J. Catal. 311 (2014) 41–51.

[2] J. He, C. Zhao, D. Mei, J.A. Lercher, Mechanisms of selective cleavage of C-O bonds in di-aryl ethers in aqueous phase, J. Catal. 309 (2014) 280–290.

[3] J. He, C. Zhao, J.A. Lercher, Ni-catalyzed cleavage of aryl ethers in the aqueous phase, J. Am. Chem. Soc. 134 (2012) 20768–20775.

[4] W. Song, Y. Liu, E. Barath, C. Zhao, J.A. Lercher, Synergistic effects of Ni and acid sites for hydrogenation and C-O bond cleavage of substituted phenols, Green Chem. 17 (2015) 1204–1218.

[5] W. Mu, H. Ben, X. Du, X. Zhang, F. Hu, W. Liu, A.J. Ragauskas, Y. Deng, Noble metal catalyzed aqueous phase hydrogenation and hydrodeoxygenation of lignin-derived pyrolysis oil and related model compounds, Bioresour. Technol. 173 (2014) 6–10.

[6] C.R. Lee, J.S. Yoon, Y.-W. Suh, J.-W. Choi, J.-M. Ha, D.J. Suh, Y.-K. Park, Catalytic roles of metals and supports on hydrodeoxygenation of lignin monomer guaiacol, Catal. Commun. 17 (2012) 54–58.

[7] D. Gao, C. Schweitzer, H.T. Hwang, A. Varma, Conversion of guaiacol on noble metal catalysts: reaction performance and deactivation studies, Ind. Eng. Chem. Res. 53 (2014) 18658–18667.

[8] J. Chang, T. Danuthai, S. Dewiyanti, C. Wang, A. Borgna, Hydrodeoxygenation of guaiacol over carbon-supported metal catalysts, ChemCatChem 5 (2013) 3041–3049.

[9] R.C. Nelson, B. Baek, P. Ruiz, B. Goundie, A. Brooks, M.C. Wheeler, B.G. Frederick, L.C. Grabow, R.N. Austin, Experimental and theoretical insights into the hydrogen-efficient direct hydrodeoxygenation mechanism of phenol over Ru/TiO2, ACS Catal. 5 (2015) 6509–6523.

[10] J. Wildschut, I. Melian-Cabrera, H. Heeres, Catalyst studies on the hydrotreatment of fast pyrolysis oil, Appl. Catal. B 99 (2010) 298–306.

[11] C. Zhao, J. He, A.A. Lemonidou, X. Li, J.A. Lercher, Aqueous-phase hydrodeoxygenation of bio-derived phenols to cycloalkanes, J. Catal. 280 (2011) 8–16.

[12] J. Sun, A.M. Karim, H. Zhang, L. Kovarik, X.S. Li, A.J. Hensley, J.-S. McEwen, Y. Wang, Carbon-supported bimetallic Pd–Fe catalysts for vapor-phase hydrodeoxygenation of guaiacol, J. Catal. 306 (2013) 47–57.

[13] A. Gutierrez, R. Kaila, M. Honkela, R. Slioor, A. Krause, Hydrodeoxygenation of guaiacol on noble metal catalysts, Catal. Today 147 (2009) 239–246.

[14] J.E. Peters, J.R. Carpenter, D.C. Dayton, Anisole and guaiacol hydrodeoxygenation reaction pathways over selected catalysts, Energy Fuels 29 (2015) 909–916.

[15] G. Yao, G. Wu, W. Dai, N. Guan, L. Li, Hydrodeoxygenation of lignin-derived phenolic compounds over bi-functional Ru/H-Beta under mild conditions, Fuel 150 (2015) 175–183.

[16] A. Sanna, T.P. Vispute, G.W. Huber, Hydrodeoxygenation of the aqueous fraction of bio-oil with Ru/C and Pt/C catalysts, Appl. Catal. B 165 (2015) 446–456.

[17] Z. Luo, Z. Zheng, Y. Wang, G. Sun, H. Jiang, C. Zhao, Hydrothermally stable Ru/HZSM-5-catalyzed selective hydrogenolysis of lignin-derived substituted phenols to bio-arenes in water, Green Chem. 18 (2016) 5845–5858.

[18] J. Lu, S. Behtash, O. Mamun, A. Heyden, Theoretical investigation of the reaction mechanism of the guaiacol hydrogenation over a Pt (111) catalyst, ACS Catal. 5 (2015) 2423–2435.

[19] K. Lee, G.H. Gu, C.A. Mullen, A.A. Boateng, D.G. Vlachos, Guaiacol hydrodeoxygenation mechanism on Pt (111): Insights from density functional theory and linear free energy relations, ChemSusChem 8 (2015) 315–322.

[20] C.-C. Chiu, A. Genest, A. Borgna, N. Rösch, Hydrodeoxygenation of guaiacol over Ru(0001): A DFT study, ACS Catal. 4 (2014) 4178–4188.

[21] J. Lu, A. Heyden, Theoretical investigation of the reaction mechanism of the hydrodeoxygenation of guaiacol over a Ru (0001) model surface, J. Catal. 321 (2015) 39–50.

[22] A.J. Hensley, Y. Wang, J.-S. McEwen, Adsorption of guaiacol on Fe (110) and Pd (111) from first principles, Surf. Sci. 648 (2016) 227–235.

[23] J. Shangguan, M.V. Olarte, Y.-H. Chin, Mechanistic insights on CO and CC bond activation and hydrogen insertion during acetic acid hydrogenation catalyzed by ruthenium clusters in aqueous medium, J. Catal. 340 (2016) 107–121.

[24] D.D. Hibbitts, B.T. Loveless, M. Neurock, E. Iglesia, Mechanistic role of water on the rate and selectivity of fischer-tropsch synthesis on ruthenium catalysts, Angew. Chem. Int. Ed. 52 (2013) 12273–12278.

[25] X. Shen, L.-J. Garces, Y. Ding, K. Laubernds, R.P. Zerger, M. Aindow, E.J. Neth, S.L. Suib, Behavior of H2 chemisorption on Ru/TiO2 surface and its application in evaluation of Ru particle sizes compared with TEM and XRD analyses, Appl. Catal. A 335 (2008) 187–195.

[26] J. He, C. Zhao, J.A. Lercher, Impact of solvent for individual steps of phenol hydrodeoxygenation with Pd/C and HZSM-5 as catalysts, J. Catal. 309 (2014) 362–375.

[27] J. Burés, Variable time normalization analysis: General graphical elucidation of reaction orders from concentration profiles, Angew. Chem. Int. Ed. 55 (2016) 16084–16087.

[28] P. Jakob, D. Menzel, Coadsorption of benzene and hydrogen on ruthenium (001), Langmuir 7 (1991) 134–139.

[29] R.C. Nelson, B. Baek, P. Ruiz, B. Goundie, A. Brooks, M.C. Wheeler, B.G. Frederick, L.C. Grabow, R.N. Austin, Experimental and theoretical insights into the hydrogen-efficient direct hydrodeoxygenation mechanism of phenol over Ru/TiO2, ACS Catal. (2015) 6509–6523.

[30] P. Jakob, D. Menzel, The adsorption of benzene on Ru(001), Surf. Sci. 201 (1988) 503–530.

[31] C. Stellwag, G. Held, D. Menzel, The geometry of ordered benzene layers on Ru (001), Surf. Sci. 325 (1995) L379–L384.

[32] W. Braun, G. Held, H.-P. Steinrück, C. Stellwag, D. Menzel, Coverage-dependent changes in the adsorption geometries of ordered benzene layers on Ru(0001), Surf. Sci. 475 (2001) 18–36.

[33] J. Shangguan, A.J.R. Hensley, J.E. Bray, M.V. Gradiski, N. Chaudhary, R.H. Morris, J.-S. McEwen, Y.-H. Chin, (Unpublished results).

[34] D. Liu, G. Li, F. Yang, H. Wang, J. Han, X. Zhu, Q. Ge, Competition and cooperation of hydrogenation and deoxygenation reactions during hydrodeoxygenation of phenol on Pt(111), J. Phys. Chem. C 121 (2017) 12249–12260.

[35] G.H. Gu, C.A. Mullen, A.A. Boateng, D.G. Vlachos, Mechanism of dehydration of phenols on noble metals via first-principles microkinetic modeling, ACS Catal. 6 (2016) 3047–3055.

[36] Q. Tan, G. Wang, L. Nie, A. Dinse, C. Buda, J. Shabaker, D.E. Resasco, Different product distributions and mechanistic aspects of the hydrodeoxygenation of m-cresol over platinum and ruthenium catalysts, ACS Catal. 5 (2015) 6271–6283.

[37] D. Liu, G. Li, F. Yang, H. Wang, J. Han, X. Zhu, Q. Ge, Competition and cooperation of hydrogenation and deoxygenation reactions during hydrodeoxygenation of phenol on Pt (111), J. Phys. Chem. C (2017).

[38] M.K. Sabbe, G. Canduela-Rodriguez, M.-F. Reyniers, G.B. Marin, DFT-based modeling of benzene hydrogenation on Pt at industrially relevant coverage, J. Catal. 330 (2015) 406–422.

[39] W.M. Haynes, CRC Handbook of Chemistry and Physics, CRC Press, 2014.

[40] S.K. Iyemperumal, N.A. Deskins, Evaluating solvent effects at the aqueous/Pt (111) interface, ChemPhysChem 18 (2017) 2171–2190.

[41] R. Bai, J. Deng, R.T. Yang, Improved multisite langmuir model for mixture adsorption using multiregion adsorption theory, Langmuir 19 (2003) 2776–2781.

[42] T. Nitta, T. Shigetomi, M. KURO-OKA, T. Katayama, An adsorption isotherm of multi-site occupancy model for homogeneous surface, J. Chem. Eng. Japan 17 (1984) 39–45.

[43] M. Boudart, G. Djéga-Mariadassou, Kinetics of Heterogeneous Catalytic Reactions, Princeton University Press, 2014.

[44] D. Gocmen, A. Elston, T. Williams, M. Parish, R. Rouseff, Identification of medicinal off-flavours generated by Alicyclobacillus species in orange juice using GC–olfactometry and GC–MS, Lett. Appl. Microbiol. 40 (2005) 172–177.

[45] P.R. Pérez-Cacho, M.D. Danyluk, R. Rouseff, GC–MS quantification and sensory thresholds of guaiacol in orange juice and its correlation with Alicyclobacillus spp, Food Chem. 129 (2011) 45–50.

[46] E. Grunwald, M.S. Puar, Proton exchange of phenol in aqueous acid, J. Phys. Chem. 71 (1967) 1842–1845.

[47] M. Ojeda, A. Li, R. Nabar, A.U. Nilekar, M. Mavrikakis, E. Iglesia, Kinetically relevant steps and H2/D2 isotope effects in fischer-tropsch synthesis on Fe and Co catalysts, J. Phys. Chem 100 (2010) 19761–19770.

[48] K.B. Wiberg, The deuterium isotope effect, Chem. Rev. 55 (1955) 713–743.